

# The triangular vortex lattices in the Kitaev honeycomb model

A Thesis

submitted to

Indian Institute of Science Education and Research Pune  
in partial fulfillment of the requirements for the  
BS-MS Dual Degree Programme

by

Sourabh Patil



Indian Institute of Science Education and Research Pune  
Dr. Homi Bhabha Road,  
Pashan, Pune 411008, INDIA.

April, 2020

Supervisor: Dr. Jean-Noël Fuchs and Dr. Julien Vidal

© Sourabh Patil 2020

All rights reserved



# Certificate

This is to certify that this dissertation entitled *The triangular vortex lattices in the Kitaev honeycomb model* towards the partial fulfilment of the BS-MS dual degree programme at the Indian Institute of Science Education and Research, Pune represents study/work carried out by Sourabh Patil , Indian Institute of Science Education and Research under the supervision of Dr. Jean-Noël Fuchs and Dr. Julien Vidal, CNRS, LPTMC, Sorbonne University, during the academic year 2019-2020.



Dr. Jean-Noël Fuchs

Dr. Julien Vidal



Dr. Sreejith GJ

Committee:

Dr. Jean-Noël Fuchs and Dr. Julien Vidal

Dr. Sreejith GJ

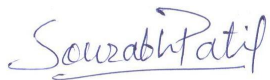


This thesis is dedicated to my beloved parents



# Declaration

I hereby declare that the matter embodied in the report entitled *The triangular vortex lattices in the Kitaev honeycomb model*, is the result of the work carried out by me at the LPTMC, Sorbonne University, under the supervision of Dr. Jean-Noël Fuchs and Dr. Julien Vidal and partly at the Indian Institute of Science Education and Research, Pune, under the supervision of Dr. Sreejith GJ and the same has not been submitted elsewhere for any other degree.

A handwritten signature in blue ink that reads "Sourabh Patil". The signature is written in a cursive style with a horizontal line underneath the name.

Sourabh Patil





# Acknowledgment

I am sincerely thankful to my supervisors Dr. Jean-Noël Fuchs and Dr. Julien Vidal at LPTMC, Sorbonne University for their constant guidance on the project as well as their all-round support throughout this journey.

I want to thank Dr. Sreejith GJ from IISER Pune for his valuable time helping me learn the basics of the Kitaev model and for the suggestions in other academic matters.

I am thankful to the LPTMC, Sorbonne University for hosting me for the duration of my project. This work was funded by Erasmus+ International Credit Mobility Grant and by the grant from LPTMC and I am very grateful towards them for the same.

I am forever indebted to the support and love from my family and friends during this time.



# Abstract

This thesis aims to study the vortex lattices in the Kitaev honeycomb model in the presence of time-reversal breaking term. The gapped spectrum in the Kitaev model is characterized by a Chern number and the system hosts anyonic excitations. This project aims at finding these 16 types of phases within the Kitaev model in the presence of triangular vortex lattices and build effective models of Majorana fermions to explain the trends.



# Contents

<b>Abstract</b>	<b>xi</b>
<b>1 Introduction</b>	<b>1</b>
<b>2 The Kitaev model</b>	<b>5</b>
2.1 The Hamiltonian in Majorana representation and the spectrum of fermions . . . . .	7
2.2 The gapless phase with $J_x = J_y = J_z$ under external magnetic field. . . . .	9
2.3 The 16-fold way . . . . .	11
<b>3 Vortex lattices: Gap as a function of <math>\kappa</math> and different phases</b>	<b>13</b>
3.1 Computational Methods . . . . .	14
3.2 Vortex free lattice . . . . .	15
3.3 Vortex-full lattice . . . . .	17
3.4 Triangular vortex lattices . . . . .	18
3.5 Symmetries of the model . . . . .	19
3.6 $\rho = \frac{1}{n}$ . . . . .	21
3.7 $\rho = \frac{n-1}{n}$ . . . . .	28
<b>4 Table of Chern numbers and observations</b>	<b>31</b>

4.1	$\rho = \frac{1}{n}$ . . . . .	31
4.2	$\rho = \frac{n-1}{n}$ . . . . .	33
4.3	Vortex densities of $\rho = 4/7, \rho = 2/7, \rho = 4/9, \rho = 6/9$ in search for the Chern numbers $\nu = \pm 7$ . . . . .	34
<b>5</b>	<b>Effective Majorana model for <math>\rho = \frac{1}{n}</math> lattices</b>	<b>35</b>
5.1	A vortex pair interaction . . . . .	35
5.2	Formation of vortex bands . . . . .	37
5.3	Hamiltonian for the effective model . . . . .	38
5.4	Validity of the effective model . . . . .	40
5.5	Obtaining hopping parameters from microscopic model . . . . .	42
<b>6</b>	<b>Effective Majorana model for <math>\rho = \frac{n-1}{n}</math> lattices</b>	<b>45</b>
6.1	$\rho = \frac{n-1}{n}$ lattices where n-1 is an even number . . . . .	46
6.2	$\rho = \frac{n-1}{n}$ lattices where n-1 is odd . . . . .	48
<b>7</b>	<b>Conclusion</b>	<b>49</b>

# Chapter 1

## Introduction

Topological matter has been a subject of massive attention and a focus of research in recent years. This can be attributed to their novel properties and their potential use in quantum computation. The topological insulators are the class of materials characterized by an insulating bulk but a presence of conducting edge states. The topological superconductors on the other hand are the superconductors with non-trivial band structure for Bogoliubov quasiparticles and have the presence of chiral Majorana edge modes. The edge modes in these type of materials are topologically protected against the perturbations to the Hamiltonian due to the the presence of symmetries within the system when the bulk gap is not closed. The phases in such materials are characterized by either an integer  $\mathbb{Z}$  or  $\mathbb{Z}_2$  numbers ( $\pm 1$ ), which are topological invariants for the corresponding phase.

The integer topological invariant is also called as Chern number. It has been previously useful in characterizing topologically ordered phases in the integer quantum Hall effect (IQHE) [17], [18]. In IQHE, the Hall conductance is quantized and it is proportional to the Chern number. As the IQHE states with different Chern numbers (different values of Hall conductivity) cannot be adiabatically connected to one another, they are distinct topological phases.

The quantum spin Hall effect [19] preserves time-reversal symmetry in contrast to the IQHE and it is characterized by the  $\mathbb{Z}_2$  topological invariant. The edge states here are Kramers pairs and the number of these edge states, odd or even, give only two distinct topological phases characterized by  $\pm 1$ .

Another example of a system with topological phases include spinless  $p_x + ip_y$  superconductor [11]. It has a particle-hole symmetry but a broken time-reversal symmetry. It has a  $\mathbb{Z}$  invariant in

two dimensions.

All such systems with topological phases can be classified in different classes depending upon the symmetries present in the system. This classification is studied earlier [7], [15] and given in table [1.1]

		TRS	PHS	SLS	$d=1$	$d=2$	$d=3$
Standard (Wigner-Dyson)	A (unitary)	0	0	0	-	$\mathbb{Z}$	-
	AI (orthogonal)	+1	0	0	-	-	-
	AII (symplectic)	-1	0	0	-	$\mathbb{Z}_2$	$\mathbb{Z}_2$
Chiral (sublattice)	AIII (chiral unitary)	0	0	$\mathbb{H}$	$\mathbb{Z}$	-	$\mathbb{Z}$
	BDI (chiral orthogonal)	+1	+1	1	$\mathbb{Z}$	-	-
	CII (chiral symplectic)	-1	-1	1	$\mathbb{Z}$	-	$\mathbb{Z}_2$
BdG	D	0	+1	0	$\mathbb{Z}_2$	$\mathbb{Z}$	-
	C	0	-1	0	-	$\mathbb{Z}$	-
	DIII	-1	+1	1	$\mathbb{Z}_2$	$\mathbb{Z}_2$	$\mathbb{Z}$
	CI	+1	-1	1	-	-	$\mathbb{Z}$

Figure 1.1: Ten symmetry classes of single-particle Hamiltonians classified in terms of the presence or absence of time-reversal symmetry, particle-hole symmetry and sublattice symmetry. Figure taken from Ref [7]

In a slightly different context, there exist frustrated magnetic systems where spins are highly correlated to each other and their unique feature is the absence of symmetry breaking or absence of order even at low temperatures [16]. The thermal fluctuations restrict ordering due to the presence of a large number degenerate states. A simple example of this is a triangular lattice with antiferromagnetic interaction which favour anti-parallel alignment of spins. All three spins on a triangle cannot be anti-parallel to each other at the same time which makes them frustrated and it leads to a number (six, here) of degenerate ground states. There can be a number of ways to obtain frustration including geometric frustration and other exchange interactions.

Frustrated magnets can form "spin liquids" when the interacting spins do not break any symmetry even at absolute zero temperature. The main feature of a Quantum spin liquid (QSL) that distinguishes them from classical spin liquids is the presence of long-range entanglement [16]. They are good examples of entangled quantum matter and have exotic topological properties. A subclass of QSLs is Kitaev Spin liquid [1] which has Ising-like exchange interaction depending



upon the type of link in the honeycomb lattice. The Kitaev model can be also thought as free Majorana fermions in the presence of  $Z_2$  gauge field. There can be  $\pi$  fluxes in the system called as "vortices". The Kitaev honeycomb model is a widely studied system, unique due to its exact solvability, a variety of gapped and gapless phases and non-abelian excitations in presence of the perturbations.

It can be shown that the Kitaev model in presence of time-reversal breaking term describes a 2D chiral topological superconductor. The latter is classified by a Chern number as it belongs to the  $D$  class of the 10-fold way, see table 1.1.

The  $Z_2$  gauge theory coupled to Majorana fermions with gapped spectrum and Chern number  $\nu$  give rise to a variety of "topological orders". Topological order is a useful concept in classifying gapped phases which are beyond Landau's formalism of phase transitions. The topological order has an important feature; the presence of fractionalized fundamental particles into quasiparticles which have non-local behaviour. These fractionalized quasiparticles also known as "anyons" possess exotic exchange statistics in  $2D$  which are different than fermions or bosons. The process of braiding two anyons around each other makes a non-trivial change in the quantum state, on a single quantum state for abelian anyons and on a degenerate space for non-abelian anyons. Each topological order is different based on the topological properties of anyonic excitations, different classes of anyons and the braiding and fusion rules between them.

In the Kitaev model, although there can be infinite number of edge theories having Majorana edge modes, there are only 16 classes of vortex-fermion statistics in the bulk depending upon  $\nu \bmod 16$ . If  $\nu$  is odd, then the vortices behave as non-abelian anyons and if  $\nu$  is even, then the vortices behave as abelian anyons.

The Chern numbers found in Kitaev model can be grouped into 16 different classes. Although the recent study [8] has found 10 distinct Chern numbers, the exploration regarding 16 classes of Chern numbers have not been complete yet. We aim to complete the 16-fold way in the honeycomb model by systematically studying the triangular vortex lattices. We have managed to find 14 such classes by studying the triangular lattices. We also have arguments to show that only these 14 classes exist in triangular vortex lattices. The presence and absence of different symmetries in the system also give us important insights about the spectrum of fermions and the trends in Chern numbers. Using symmetry arguments we will show that any periodic lattice with odd number of vortices in the geometrical unit cell have only even Chern numbers. This is an important result.

To explain the patterns of Chern numbers found in these triangular vortex lattices, we build effective low energy models for Majorana fermions. The effective model for a family of triangular lattices was already studied in [2] based on the result that unpaired Majorana modes appear at the vortex cores when  $\nu$  is odd. Our work introduces the effective models for the family of antivortex (absence of vortex) lattices using the  $p_x + ip_y$  superconductivity on a triangular lattice and explain the observed phases based on these models.

# Chapter 2

## The Kitaev model

Kitaev's honeycomb model [1] describes a spin 1/2 system where the spins are located at the vertices of a honeycomb lattice and these spins have Ising like interaction with the nearest neighbour. The important feature of this model is that the spins are coupled via an interaction that depends upon the type of link. This is such that for spins  $j$  and  $k$ , the interaction term is given by  $J_{\alpha_{jk}} \sigma_j^{\alpha_{jk}} \sigma_k^{\alpha_{jk}}$  where  $\alpha_{jk} = x, y, z$ . The Hamiltonian is given by

$$H = -J_x \sum_{x\text{-links}} \sigma_j^x \sigma_k^x - J_y \sum_{y\text{-links}} \sigma_j^y \sigma_k^y - J_z \sum_{z\text{-links}} \sigma_j^z \sigma_k^z \quad (2.1)$$

where  $\sigma_j^x$ ,  $\sigma_j^y$  and  $\sigma_j^z$  are the Pauli matrices for the spin at site  $j$ . As shown in the figure [2.1], there are two sub-lattices in the system, one with a triangular lattice of black sites and the other with a triangular lattice of white sites. Each spin in the black sub-lattice is coupled to three other spins from the white sub-lattice and vice-versa.

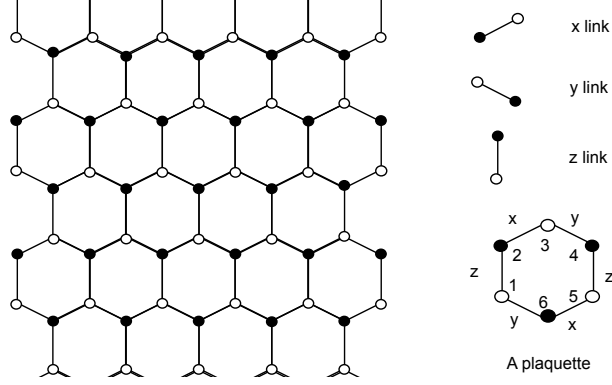


Figure 2.1: The honeycomb lattice, three types of links and a plaquette

The dimension of the Hilbert space  $\mathcal{L}$  for the Hamiltonian is given by

$$Dim(\mathcal{L}) = 2^N \quad (2.2)$$

where  $N$  is the number of spins on the lattice. It can be seen that the Hilbert space grows exponentially with the number of spins in the system and one needs to diagonalize a huge matrix to get the spectrum. Although at this moment the problem seems very difficult to solve, the constants of motion make the problem easier. The plaquette operator  $W_p$  for each hexagonal plaquette  $p$  as shown in the figure [2.1] is defined as,

$$W_p = \sigma_1^x \sigma_2^y \sigma_3^z \sigma_4^x \sigma_5^y \sigma_6^z \quad (2.3)$$

where  $\alpha = x, y, z$  depending upon the type of link. It appears that the plaquette operators commute with the Hamiltonian and with other plaquette operators;  $[W_p, H] = 0$  and  $[W_p, W_q] = 0$ . This makes the Hamiltonian block diagonal and it can be diagonalized within that subspace. In other words, the Hilbert space  $\mathcal{L}$  of the Hamiltonian, can be separated into sectors  $\mathcal{L}_{w_1, w_2, \dots, w_m}$  - set of eigenvalues of corresponding  $W_p$ .

$$\mathcal{L} = \bigoplus_{w_1, w_2, \dots, w_m} \mathcal{L}_{w_1, w_2, \dots, w_m} \quad (2.4)$$

where  $M$  is the number of plaquettes. A  $W_p$  has eigenvalues of  $\pm 1$ . If  $w_p = -1$  then the plaquette contains a  $\pi$  flux which is called a "vortex". If  $w_p = +1$  then there is no vortex. Each sector in Hilbert space will have corresponding set of values  $w_1, w_2, \dots, w_m$  where each  $w_i = \pm 1$ . This simplifies the problem to a great extent as the spectrum of the Hamiltonian can be found only in the restricted Hilbert space  $\mathcal{L}_{w_1, w_2, \dots, w_m}$  called a "vortex sector".

If number of spins in the system is  $N$ , then number of plaquettes in the system is  $M = N/2$ . The dimension of the Hilbert space is  $Dim(\mathcal{L}) = 2^N = 2^{N/2} \times 2^{N/2} = 2^M \times 2^M$ . Therefore each sector has a dimension of  $2^M$  and number of such sectors is  $2^M$ . Although there has been a huge reduction in the dimension of Hilbert space of each sector, it is exponentially increasing with  $M$ . However, as we will further see, a transformation of spins to Majorana fermions problem can be done which then can be solved exactly!

## 2.1 The Hamiltonian in Majorana representation and the spectrum of fermions

Majorana fermion is a type of fermion which is its own antiparticle. It was introduced by Ettore Majorana in 1937 [14]. Majoranas appear as quasiparticles in condensed matter physics especially in superconducting systems and constructed as excitations made as superpositions of electron and hole. Majorana fermions  $c_j$ , which are the linear combinations of the usual complex fermionic operators  $a_j$  and  $a_j^\dagger$ , can also be used to describe a system with fermionic modes.

$$c_{2k-1} = a_k + a_k^\dagger, \quad c_{2k} = i(a_k^\dagger - a_k) \quad (2.5)$$

$$c_j^2 = 1, \quad c_j c_k = -c_k c_j \quad \text{if } j \neq k \quad (2.6)$$

A spin 1/2 of dimension 2 can be represented by 2 complex fermions in the Fock space, by representing a spin up by no fermion state and spin down by two fermion state. As each complex fermion corresponds to 2 Majorana fermions, each spin is represented by 4 Majorana fermions  $b^x, b^y, b^z, c$  such that

$$\tilde{\sigma}^{\alpha_j} = i b_j^\alpha c_j \quad (2.7)$$

Majorana fermions  $b^x, b^y, b^z, c$  can be written in terms of complex fermions using equation [2.5]

$$a_1 + a_1 = b^x \quad (2.8)$$

$$i(a_1^\dagger - a_1) = b^y \quad (2.9)$$

$$a_2 + a_2 = b^z \quad (2.10)$$

$$i(a_2^\dagger - a_2) = c \quad (2.11)$$

The Pauli operators  $\tilde{\sigma}^{\alpha_j}$  act on the extended space  $\tilde{\mathcal{L}}$ . Each Majorana fermion  $c_j$  has a Hilbert space of the dimension  $\sqrt{2}$ . Therefore the Hilbert space for 4 Majorana fermions becomes  $\sqrt{2}^4 = 4$  while a single spin has the Hilbert space of 2. This makes the dimension of the Hilbert space much larger than the original one,  $2^{2N}$  instead of  $2^N$ . Therefore, to project states from the extended space with 4 Majoranas to the physical states with spins, we need a projection operator.

$$D_j = b_j^x b_j^y b_j^z c_j \quad (2.12)$$

The operator  $D$  satisfies  $D|\psi\rangle = |\psi\rangle$  if and only if  $|\psi\rangle$  belongs to the physical space.

After replacing the spin operators by Majorana operators and defining the  $Z_2$  gauge field  $\hat{u}_{jk} = ib_j^\alpha b_k^\alpha$  and  $\hat{u}_{kj} = -\hat{u}_{jk}$ , the Hamiltonian can be written as

$$\tilde{H} = \frac{i}{2} \sum_{j,k} J_{\alpha_{jk}} \hat{u}_{jk} c_j c_k \quad (2.13)$$

Note that  $\alpha$  takes a value from  $x, y, z$  depending upon the type of link. It appears that the link operators commute with the Hamiltonian and with the other link operators;  $[\hat{u}_{jk}, H] = 0$  and  $[\hat{u}_{jk}, \hat{u}_{lm}] = 0$ . Therefore the eigenspaces of the Hilbert space  $\tilde{\mathcal{L}}$  can be characterized by the eigenvalues of  $\hat{u}_{jk} \pm 1$ . So just like before, the Hilbert space  $\tilde{\mathcal{L}}$  can be split into sectors

$$\tilde{\mathcal{L}} = \bigoplus_u \tilde{\mathcal{L}}_u \quad (2.14)$$

This means we can replace operators  $\hat{u}_{jk}$  by  $u_{jk} = \pm 1$  making the Hamiltonian to be

$$\tilde{H} = \frac{i}{2} \sum_{j,k} J_{\alpha_{jk}} u_{jk} c_j c_k \quad (2.15)$$

This is a quadratic Hamiltonian and corresponds to a free Majorana fermion problem. Thus we have transformed a difficult spin problem into a easy free fermion problem. The cost for this is that there are now multiple easy problems (corresponding to each vortex sector) to solve rather than a single difficult problem. The ground state of the above Hamiltonian can be found by writing it into the canonical form

$$\tilde{H} = i \sum_{k=1}^m \varepsilon_k b'_k b''_k = \sum_{k=1}^m \varepsilon_k (2a_k^\dagger a_k - 1) \quad (2.16)$$

where  $b'_k$  and  $b''_k$  are normal modes and  $a_k^\dagger = b'_k - ib''_k$  and  $a_k = b'_k + ib''_k$ . Thus, the ground state satisfies the condition  $a_k |\psi\rangle = 0$  for all  $k$ . The spectrum of the matrix  $iA$  (where  $A_{jk} = J_{\alpha_{jk}} u_{jk}$ )

gives us the values  $\pm\varepsilon$ . Therefore the ground state energy is

$$E = -\sum_{k=1}^m \varepsilon_k = -\frac{1}{2}\text{Tr}|iA| \quad (2.17)$$

The ground state energy is different with different choices of  $u_{jk}$ . According to Lieb's theorem, the vortex-free sector where  $u_{jk} = 1$  where  $j$  belongs to one sublattice and  $k$  belongs to the other sublattice, hosts the overall ground state. The spectrum  $\varepsilon(q)$  for the vortex-free sector, where  $\mathbf{a}_1 = (\frac{1}{2}, \frac{\sqrt{3}}{2})$ ,  $\mathbf{a}_2 = (-\frac{1}{2}, \frac{\sqrt{3}}{2})$  is given by

$$\varepsilon(q) = \pm|f(q)|, \quad f(q) = 2(J_x e^{iq \cdot \mathbf{a}_1} + J_y e^{iq \cdot \mathbf{a}_2} + J_z) \quad (2.18)$$

If there exist  $q$  such that  $\varepsilon(q) = 0$  then the spectrum is gapless. For vortex free case to be gapless, we need  $J_x e^{iq \cdot \mathbf{a}_1} + J_y e^{iq \cdot \mathbf{a}_2} + J_z = 0$ . This equation is satisfied if and only if the following triangle inequalities hold true:

$$|J_x| \leq |J_y| + |J_z|, \quad |J_y| \leq |J_x| + |J_z|, \quad |J_z| \leq |J_x| + |J_y| \quad (2.19)$$

## 2.2 The gapless phase with $J_x = J_y = J_z$ under external magnetic field.

We will restrict our study of Kitaev model to the  $J_x = J_y = J_z$  case from now on. Kitaev [1] had already shown that the perturbation of the type  $V = -\sum_j (h_x \sigma_j^x + h_y \sigma_j^y + h_z \sigma_j^z)$  acting on the vortex-free sector where  $\mathbf{h} = (h_x, h_y, h_z)$  is a magnetic field, open up the gap. In the perturbation theory study to build an effective Hamiltonian  $H_{eff}$ , one can see that the first order term  $H_{eff}^{(1)} = 0$ . The second order term  $H_{eff}^{(2)} \neq 0$ , but it fails to break time-reversal symmetry. The third order term

$$H_{eff} \sim -\frac{h_x h_y h_z}{J^2} \sum_{j,k,l} \sigma_j^x \sigma_k^y \sigma_l^z \quad (2.20)$$

indeed breaks time-reversal symmetry and opens up the gap. We identify  $\kappa \sim \frac{h_x h_y h_z}{J^2}$ . In the language of Majorana operators, the Hamiltonian becomes quadratic, given by

$$H = \frac{i}{2} J \sum_{j,k} u_{jk} c_j c_k - i\kappa \left( \sum_{l,k,j} u_{jk} u_{kl} c_j c_l + h.c. \right) \quad (2.21)$$

where  $(l,k,j)$  represents a triplet of connected sites oriented anticlockwise.

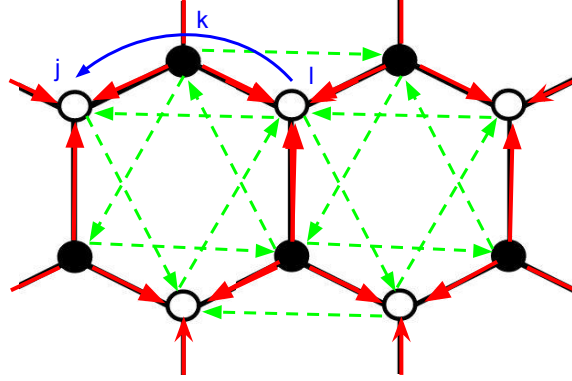


Figure 2.2: The first and the second nearest neighbour hoppings for Majorana fermions shown in red and green respectively. A triplet of sites in an anticlockwise direction shown in blue.

The  $\kappa$  term breaks time reversal symmetry and opens the gap for the vortex-free lattice. Similarly, other vortex sectors also appear gapped after introducing the  $\kappa$  term. As  $\kappa$  is varied there are multiple gapped phases separated by a gapless point or an extended gapless phase. Each of these gapped phases can be characterized by a Chern number  $\nu$ . The Chern number is a topological invariant of these gapped phases. It is defined as

$$\nu = \frac{1}{2\pi i} \int Tr \left( P \left( \frac{\partial P}{\partial q_x} \frac{\partial P}{\partial q_y} - \frac{\partial P}{\partial q_y} \frac{\partial P}{\partial q_x} \right) \right) dq_x dq_y \quad (2.22)$$

where  $P = \sum_n |u_n(\mathbf{q})\rangle \langle u_n(\mathbf{q})|$  where the energy  $\epsilon_n < 0$ , is the projector on the filled negative energy bands. The  $u_n(\mathbf{q})$  are the eigenstates corresponding to the filled negative energy bands with band index  $n$ . The number of edge modes in the system is also equal to the Chern number. One should note that the edge modes in the Kitaev model carry only the thermal energy and not the electric



current (as seen in quantum Hall effect). This can be attributed to the real modes which constitute the edge transport in Kitaev model in contrast to the complex modes in quantum Hall effect.

## 2.3 The 16-fold way

Topological order is a useful concept in classifying gapped phases beyond Landau's formalism of spontaneous symmetry breaking. Each topological order is different based on the topological properties of anyonic excitations, different classes of anyons and the braiding and fusion rules between them.

In the Kitaev model, the  $\mathbb{Z}_2$  gauge theory coupled to Majorana fermions with gapped spectrum and Chern number  $\nu$  give rise to a variety of topological orders. Although there can be infinite number of edge theories having Majorana edge modes, there are only 16 classes of vortex-fermion statistics in the bulk depending upon  $\nu \bmod 16$ . If  $\nu$  is odd, then the vortices behave as non-abelian anyons and if  $\nu$  is even, then the vortices behave as abelian anyons.

If  $\nu$  is odd, then each vortex carries an unpaired Majorana mode [1]. A pair of Majorana modes in two vortices constitute a complex fermionic mode. The state of such a pair is protected from perturbations and measurements as long as the vortices stay far away from each other. The vortex carrying a MZM is one superselection sector  $\sigma$  along with 1 (vacuum) and  $\varepsilon$  (fermion). The fusion rules (splitting rules if read backward) are given as

$$\varepsilon \times \varepsilon = 1 \tag{2.23}$$

which indicates two fermions annihilating each other upon fusion.

$$\varepsilon \times \sigma = \sigma \tag{2.24}$$

which indicates that a fermion and a vortex leave behind a vortex after fusion.

$$\sigma \times \sigma = 1 + \varepsilon \tag{2.25}$$

which indicates that two vortices can fuse to either annihilate or give a fermion. The braiding rules for anyons are very specific to the topological order. These are described in detail along with the associativity relations in ref [1].

If  $\nu$  is even, then there are no unpaired MZM with the vortex. This means there are two different classes as a vortex cannot absorb fermion and stay in the same superselection sector. If  $\nu \bmod 4 = 0$ , then the vortices are indicated as  $e$  and  $m$  and the fusion rules are

$$\varepsilon \times e = m, \quad \varepsilon \times m = e, \quad e \times m = \varepsilon \quad (2.26)$$

If  $\nu \bmod 4 = 2$ , then the vortices are indicated as  $a$  and  $\tilde{a}$  and the fusion rules [1] are

$$a \times \varepsilon = \tilde{a}, \quad \tilde{a} \times \varepsilon = a, \quad \varepsilon \times \varepsilon = 1, \quad a \times a = \tilde{a} \times \tilde{a} = \varepsilon, \quad a \times \tilde{a} = 1 \quad (2.27)$$

Associativity relations and braiding rules can be found as shown in [1].

In the next chapter, we explore the triangular vortex lattices to find a variety of gapped phases and find the Chern number associated with each of them. The knowledge of Chern number would be useful in knowing which topological order appears in a particular vortex sector and if we can find each of these 16 classes of anyons.

## Chapter 3

# Vortex lattices: Gap as a function of $\kappa$ and different phases

A vortex sector is defined by a particular arrangement of vortices ( $w_p = -1$ ) in the system. For example, if  $w_p = 1$  for all plaquettes  $p$  in the system, then the system is said to be in the vortex-free sector. On the other hand, if  $w_p = -1$  for all plaquettes  $p$  in the system, then the system is said to be in the vortex-full sector. A vortex lattice for example can be constructed with periodic arrangement of the vortices in the system. The simplest vortex lattices that can be studied are the triangular vortex lattices. We aim to study these triangular vortex lattices by characterising the phases in each triangular vortex lattice, computing the gap as a function of  $\kappa$ , Chern numbers and try to explain the patterns in Chern numbers using the effective models based on Majorana fermions.

It is interesting to find the behavior of gap as external magnetic field  $\kappa$  is switched on and increased. For each vortex configuration, the plot of the gap as a function of  $\kappa$  would be helpful in observing different phases (gapped or gapless) that occur with  $\kappa$ .

## 3.1 Computational Methods

### 3.1.1 Chern number

The Chern number formula involving the projectors is defined in 2.22. To compute the projectors, one needs to compute  $u_n(\mathbf{k})$  which in turn are obtained by diagonalizing the Hamiltonian 2.21 using Fourier transformation.

For the vortex-free sector which has only two bands, the Chern number can be found analytically [1],  $\nu = \pm 1$  depending upon the direction of the magnetic field. To compute the Chern number for vortex-full sector having four bands or other vortex configurations with more than 2 bands, we need to use numerical approaches as analytical approach is not possible.

In order to numerically compute the Chern number using 2.22, we need to discretize the Brillouin zone and compute a discretized version of the formula 2.22 involving the projector onto the occupied states. The projector onto the occupied states is obtained from the numerically obtained eigenvectors which in turn is obtained by diagonalizing the hamiltonian. We would also have to compute discretized gradients of this projector. The calculation is done taking  $\mathbf{k} = a\mathbf{k}_1 + b\mathbf{k}_2$  where  $\mathbf{k}_1$  and  $\mathbf{k}_2$  are the reciprocal lattice vectors. The BZ can then be chosen to be  $\mathbf{k} = a\mathbf{k}_1 + b\mathbf{k}_2$  such that  $a$  and  $b$  are in between 0 and 1. It means that we integrate over  $a$  and  $b$  (rather than over  $k_x$  and  $k_y$ ) and also that the gradients of the projector are taken with respect to  $a$  or  $b$  (rather than  $k_x$  or  $k_y$ ).

When we discretize the BZ, the numerically computed Chern number will not be an integer (because we take only a finite number of points in BZ to reduce the computational cost) but it should converge toward an integer when the grid becomes denser. Typically we start with a grid of 12 x 12 and then increase the grid size until the Chern number converges to an integer.

The ref [12] explains how to compute a topological index associated with the process of closing a band gap. This gives us the change in Chern number across  $\mathbf{k} = (k_{cx}, k_{cy})$  and across  $\kappa_c$  where the gap closing is at  $\mathbf{k} = (k_{cx}, k_{cy})$  in the momentum space and  $\kappa_c$  in  $\kappa$  space. This formula is similar to that for the charge of the 3D topological defect (for example a Weyl point). The topological index is like a Chern number (i.e. integral of a Berry curvature over a closed manifold) but the closed manifold is here a sphere  $S^2$  embedded in  $R^3$ , rather than a torus  $T^2 = BZ$ . This is like a 3D computation because in addition to  $k_x$  and  $k_y$ , there is the parameter ( $\kappa$ ) realizing the gap closing which is treated as if it was  $k_z = \kappa - \kappa_c$ . Suppose  $\mathbf{q} = (k_x - k_{cx}, k_y - k_{cy}, \kappa - \kappa_c)$ , then using

spherical co-ordinates,  $\mathbf{q} = q(\sin \theta \cos \phi, \sin \theta \sin \phi, \cos \theta)$ / The change in Chern number is then give by

$$\Delta\nu = \frac{1}{2\pi i} \int_{S^2} Tr[P(\frac{\partial P}{\partial \theta} \frac{\partial P}{\partial \phi} - \frac{\partial P}{\partial \phi} \frac{\partial P}{\partial \theta})]d\theta d\phi \quad (3.1)$$

There might be other gap closings within the vicinity of  $\kappa_c$  and also some other gap closings in the BZ. Therefore, the radius of the sphere should be such that it encloses only a single defect. When there are multiple gap closings in BZ, we add the charges of all the gap closings. This index ( $\Delta\nu$ ) is useful in confirming the Chern numbers found earlier by checking that  $\Delta\nu$  indeed matches the  $\nu_2 - \nu_1$  across a gapless point.

### 3.1.2 Gap as a function of $\kappa$

Another quantity that we compute for different vortex sectors is the value of the gap ( $\Delta$ ) with respect to  $\kappa$ . This gap is the energy difference between the states of lowest positive energy ( $E_1$ ) and the highest negative energy ( $-E_1$ ). It is usually  $\Delta = E_1 - (-E_1) = 2E_1$ . For a fixed value of  $\kappa$ , one needs to scan the whole BZ in order to identify the position  $(k_{mx}, k_{my})$  where the gap is the lowest. This can be again done numerically either by using in-built minimize function or computing the gap at a large number of points in BZ and then comparing it to find the minimum.

## 3.2 Vortex free lattice

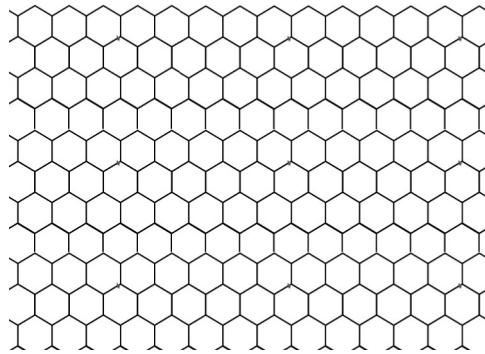


Figure 3.1: Vortex-free lattice

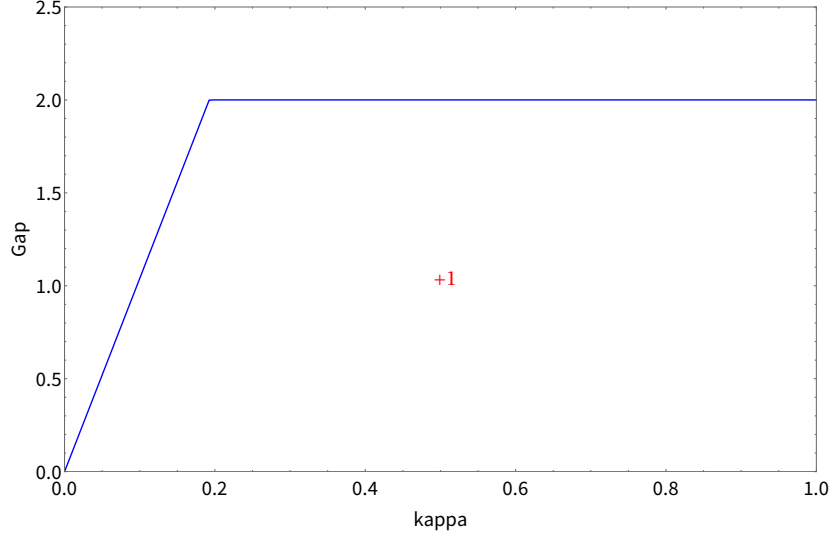


Figure 3.2: Gap as a function of  $\kappa$  for the vortex-free case. Chern numbers are indicated in red.

In his work [1], Kitaev has shown that the spectrum for the vortex-free configuration is gapless at  $\kappa = 0$  with two Dirac cones, one at  $\frac{1}{3}\mathbf{q}_1 + \frac{2}{3}\mathbf{q}_2$  and another at  $\frac{2}{3}\mathbf{q}_1 + \frac{1}{3}\mathbf{q}_2$  where  $\mathbf{q}_1$  and  $\mathbf{q}_2$  are the reciprocal lattice vectors associated with  $\mathbf{a}_1 = (1/2, \sqrt{3}/2)$  and  $\mathbf{a}_2 = (-1/2, \sqrt{3}/2)$  respectively. However, the gap opens at infinitesimal kappa. As soon as kappa is different from zero, the gap opens up in this sector. The system remains gapped as we increase  $\kappa$ . The gap can be written as follows

$$\Delta = \min(6\sqrt{3}\kappa, 2) \quad (3.2)$$

At large  $\kappa$  the gap saturates to the value of 2. In the large  $\kappa$  behavior where  $\frac{J}{\kappa} \rightarrow 0$ , there is only a next-nearest neighbour hopping present as the nearest neighbour hopping corresponding to  $J$  term in the Hamiltonian is negligible. Thus we get two decoupled triangular lattices as shown in the figure. The Chern number for this gapped phase is

$$v_0 = +1, \quad \text{for } \kappa > 0 \quad (3.3)$$

The Chern number changes its sign when the external magnetic field is reversed  $v_0 = -1$ , for  $\kappa < 0$ .

### 3.3 Vortex-full lattice

The vortex-full sector was studied earlier [5]. The spectrum contains four bands and it is gapless at  $\kappa = 0$  with four Dirac cones, at  $K_{f1} = \frac{5}{12}\mathbf{v}_1 + \frac{1}{6}\mathbf{v}_2$ ,  $K_{f2} = -(\frac{5}{12}\mathbf{v}_1 + \frac{1}{6}\mathbf{v}_2)$ ,  $K_{f3} = \frac{1}{12}\mathbf{v}_1 - \frac{1}{6}\mathbf{v}_2$  and at  $K_{f4} = -(\frac{1}{12}\mathbf{v}_1 - \frac{1}{6}\mathbf{v}_2)$  where  $\mathbf{v}_1$  and  $\mathbf{v}_2$  are the reciprocal lattice vectors associated with  $\mathbf{a}_1$  and  $2(\mathbf{a}_1 - \mathbf{a}_2)$  respectively.

The Chern numbers for the two gapped phases can be computed exactly and they are

$$v_1^a = +2 \quad \text{for } 0 < \kappa < 1/2, \quad (3.4)$$

$$v_1^b = -2 \quad \text{for } \kappa > 1/2, \quad (3.5)$$

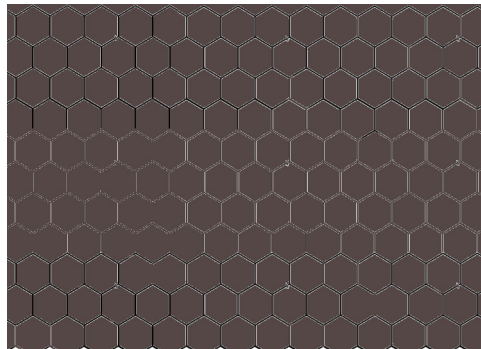


Figure 3.3: Vortex-full case

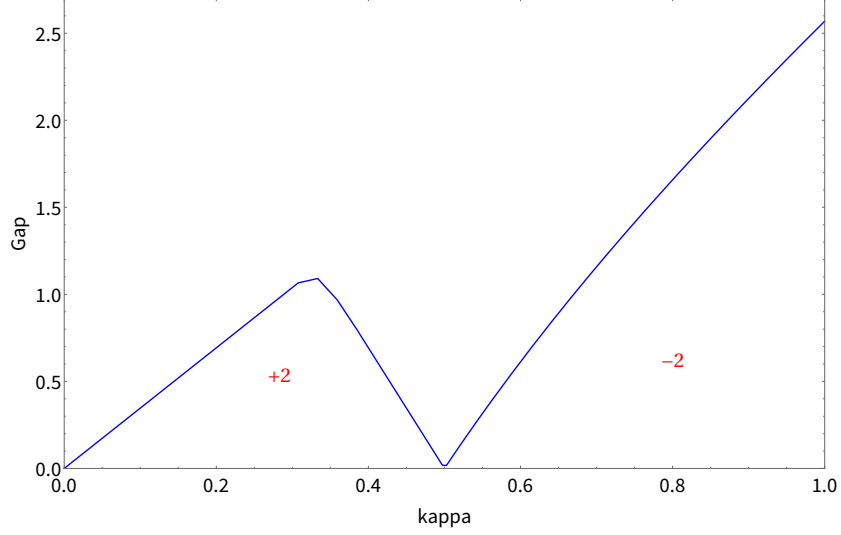


Figure 3.4: Gap as a function of  $\kappa$  for the vortex-full case. Chern numbers are indicated in red.

### 3.4 Triangular vortex lattices

As the vortex free sector has no vortex present in the system, the vortex density  $\rho$  is 0. On the other hand, the vortex-full sector has 1 vortex in each plaquette, therefore the vortex density  $\rho$  is 1. We aim to study the intermediate vortex densities where  $0 < \rho < 1$  and characterize the phases as we change  $\kappa$ . There can be a number of vortex arrangements like triangular, striped, random etc giving the same vortex density. We explore only the triangular lattices and their duals (obtained by changing the sign of  $w_p$  in all the plaquettes) in our work. We summarize our work of each triangular vortex lattice by studying the gap as a function of  $\kappa$  and the Chern numbers.

The triangular vortex lattices can be constructed by specifying two integers  $p$  and  $q$  which define the unit cell vectors of the “geometrical unit cell”. The geometrical unit cell is obtained solely from considering the pattern of white and black plaquettes. These integers define the unit cell vectors  $\mathbf{A}_1$  and  $\mathbf{A}_2$  of such vortex lattices.

$$\mathbf{A}_1 = (p \mathbf{a}_1 + \mathbf{a}_2) \quad (3.6)$$

$$\mathbf{A}_2 = -q \mathbf{a}_1 + (p + q) \mathbf{a}_2 \quad (3.7)$$

where  $\mathbf{a}_1$  and  $\mathbf{a}_2$  are the reciprocal lattice vectors for the honeycomb lattice. The distance scale we



take is  $a = |\mathbf{a}_1| = |\mathbf{a}_2| = 1$

The triangular vortex lattices of intermediate density can then be classified into two families as given below:

$$\rho = \frac{1}{n} = \frac{1}{p^2 + pq + q^2} \quad (3.8)$$

This family of lattices is characterized by the presence of vortex superlattice (black plaquettes) on top of the vortex-free background (white plaquettes).

$$\rho = \frac{n-1}{n} = 1 - \frac{1}{p^2 + pq + q^2} \quad (3.9)$$

This family of lattices is characterized by the antivortex superlattice (absence of vortex or white plaquettes) on top of the vortex-full background (black plaquettes).

When  $\rho = \text{even}/n$ , the geometrical unit cell is same as the unit cell of the Majorana Hamiltonian. This includes the lattices with  $\rho = \frac{(n-1)}{n}$  where  $n$  is odd. When  $\rho = \text{odd}/n$ , we need to double the unit cell as the vortices are created only in pairs in a finite system with PBC. The unit cell for the Majorana Hamiltonian is twice larger than the geometrical unit cell. The unit cell vectors are given as

$$\mathbf{A}_1 = 2(p \mathbf{a}_1 + \mathbf{a}_2) \quad (3.10)$$

$$\mathbf{A}_2 = -q \mathbf{a}_1 + (p+q)\mathbf{a}_2 \quad (3.11)$$

This case includes the lattices of the type  $\rho = 1/n$  and  $\rho = \frac{(n-1)}{n}$  where  $n$  is even.

### 3.5 Symmetries of the model

The Hamiltonian 2.21 containing both  $J$  and  $\kappa$  terms can be diagonalized in momentum space for each triangular vortex lattice. It has the presence of translation symmetry, particle-hole symmetry but no time-reversal symmetry. We get a Bloch Hamiltonian  $H(\mathbf{k})$  due to the translation symmetry.

It can be written as  $H(\mathbf{k}) = i\tilde{A}(\mathbf{k})/2$  where  $\tilde{A}$  is a Fourier transform of the real skew-symmetric matrix such that  $\tilde{A}(-\mathbf{k}) = \tilde{A}(\mathbf{k})^*$ . This is because of the particle-hole symmetry which is an artificial symmetry arising due to doubling of degrees of freedom going from the spin Hamiltonian to the Majorana Hamiltonian. This is similar to what happens to the Hamiltonian of a superconductor in Bogoliubov approach. Any BdG Hamiltonian is equivalent to a quadratic Hamiltonian

for Majoranas. It means that any quadratic Hamiltonian for Majoranas has the property that the spectrum comes in  $\pm E$  pairs. Therefore, the spectrum for  $H(\mathbf{k})$  is given by  $\pm \varepsilon_n(\pm \mathbf{k})$  where  $n$  is the band index and  $0 \leq \varepsilon_1 \leq \varepsilon_2 \dots \leq \varepsilon_{N/2}$  where  $N$  is the number of spins. The particle-hole symmetry operator  $C$  is an antiunitary operator with  $C^2 = 1$ . It operates on the Hamiltonian to give  $CHC^{-1} = H(-\mathbf{k})^* = -H(\mathbf{k})$  which means that a state with energy  $\varepsilon_n(\mathbf{k})$  is sent to a state with energy  $-\varepsilon_n(-\mathbf{k})$  by the operator  $C$ . If the Hamiltonian also has an inversion symmetry, it means that  $\varepsilon_n(-\mathbf{k}) = \varepsilon_n(\mathbf{k})$ . As a consequence of both the symmetries:  $\varepsilon_n(\mathbf{k})$  becomes  $-\varepsilon_n(\mathbf{k})$ .

In any type of periodic vortex lattice, due to translation symmetry we can use the Bloch's theorem. We get  $\varepsilon_n(\mathbf{k}) = \varepsilon_n(\mathbf{k} + m\mathbf{A}_1^* + n\mathbf{A}_2^*)$  where  $\mathbf{A}_1^*$  and  $\mathbf{A}_2^*$  are the reciprocal lattice vectors corresponding to the lattice in consideration with lattice vectors  $\mathbf{A}_1$  and  $\mathbf{A}_2$ . This happens because of the magnetic translation operators  $\mathcal{T}_{\mathbf{A}_1}$  and  $\mathcal{T}_{\mathbf{A}_2}$  which commute with the Hamiltonian and with themselves. However, this is true only for the unit cell having zero flux or even number of vortices.

For any vortex lattice having  $\rho = \text{odd}/n$ , the unit cell has an odd number of vortices leading to doubling of the unit cell. Although the magnetic translation operators  $\mathcal{T}_{\mathbf{A}_1}$  and  $\mathcal{T}_{\mathbf{A}_2}$  commute, the operators  $\mathcal{T}_{\mathbf{A}_1/2}$  and  $\mathcal{T}_{\mathbf{A}_2}$  anticommute (but commute with the Hamiltonian). This extra symmetry gives rise to

$$\varepsilon_n(\mathbf{k}) = \varepsilon_n(\mathbf{k} + \mathbf{A}_2^*/2) \quad (3.12)$$

This leads to the double degeneracy of the spectrum upon translation. Therefore, the number of points in momentum space where the gap vanishes come in pairs, even the four special points which are time-reversal invariant momenta (TRIM) given by  $\Gamma = 0$ ,  $X = \mathbf{A}_1^*/2$ ,  $Y = \mathbf{A}_2^*/2$ ,  $M = (\mathbf{A}_1^* + \mathbf{A}_2^*)/2$ . As the topological charge obtained around a single gapless point is always an integer, we get an even integer after considering the contribution from a pair of such gapless points. Therefore the change in Chern number when crossing a gap closing is always an even integer. This does not yet tell us how the Chern number is even. Now consider the two types of lattices:

1. The vortex lattices with gap at  $\kappa = 0$ . Time reversal symmetry is not broken at  $\kappa = 0$  and the Chern number is 0 for this gapped phase. Now we know that  $\Delta\nu = \text{even}$ . Therefore, as we increase or decrease  $\kappa$  starting from 0, we get the total Chern number to be  $\nu = 0 + \Delta\nu = \text{even}$ .
2. The vortex lattices which are gapless at  $\kappa = 0$ . The concept of Chern number does not apply to gapless phases. However we can adiabatically change the parameters  $J_x, J_y$  and  $J_z$  to reach a gapped phase where  $|J_x|, |J_y| \ll |J_z|$ . This gapped phase is time-reversal invariant so the Chern number is  $\nu = 0$  (toric code phases in ref [1]). Therefore the total Chern number would be  $\nu = 0 + \Delta\nu = \text{even}$ .

### 3.6 $\rho = \frac{1}{n}$

We can identify two subfamilies of vortex lattices in this family. These are distinguished by the nature of the gap; either  $\text{gap} > 0$  or  $\text{gap} = 0$  at  $\kappa = 0$ .

#### 3.6.1 $\rho = \frac{1}{n}$ , where $n$ is an integral multiple of 3

These type of lattices has been studied earlier at  $\kappa = 0$  in [4]. These vortex configurations have a gapped phase in the vicinity of  $\kappa = 0$  which is a time-reversal invariant point. Therefore, the Chern number is 0.

The gap opening at  $\kappa = 0$  can be explained using the coupling of Dirac cones. The vortex free lattice has a gapless band structure at  $\kappa = 0$ , due to the presence of two Dirac cones at  $\mathbf{K}_1 = \frac{1}{3}\mathbf{q}_1 + \frac{2}{3}\mathbf{q}_2$  and  $\mathbf{K}_2 = \frac{2}{3}\mathbf{q}_1 + \frac{1}{3}\mathbf{q}_2$ . The triangular vortex superlattice (for example, vortex density  $\rho = 1/3$ ) on top of the vortex-free background creates a perturbing potential which has the same periodicity as that of vortex superlattice. The reciprocal lattice vectors of the  $\rho = 1/3$  vortex lattice can give a linear combination equal to  $\mathbf{K}_1 - \mathbf{K}_2$  thereby coupling the two Dirac cones and resulting into opening of the gap. It can be further shown that for any vortex lattice satisfying [4]

$$\frac{1}{\rho} = n = 0 \pmod{3} \quad (3.13)$$

will always have the existence of reciprocal lattice vectors whose linear combination is equal to  $\mathbf{K}_1 - \mathbf{K}_2$ .

However, as  $\kappa$  is increased, several gap closings can be observed giving rise to several gapped phases with a Chern number. In this type of vortex configurations, the vortex densities include  $\rho = \frac{1}{3}, \frac{1}{9}, \frac{1}{12}, \dots$  and so on.

For the vortex density of  $\rho = \frac{1}{3}$ , one can observe that there are five points where the gap vanishes giving rise to six gapped phases as listed below.

$$v_{1/3}^a = 0, \text{ for } 0 < \kappa < 0.224745, \quad (3.14)$$

$$v_{1/3}^b = +4, \text{ for } 0.224745 < \kappa < 0.242614, \quad (3.15)$$

$$v_{1/3}^c = -2, \text{ for } 0.242614 < \kappa < 0.313859, \quad (3.16)$$

$$v_{1/3}^d = +2, \text{ for } 0.313859 < \kappa < 2.22474, \quad (3.17)$$

$$v_{1/3}^e = -2, \text{ for } 2.22474 < \kappa < 3.18614, \quad (3.18)$$

$$v_{1/3}^f = -6, \text{ for } \kappa < 3.18614, \quad (3.19)$$

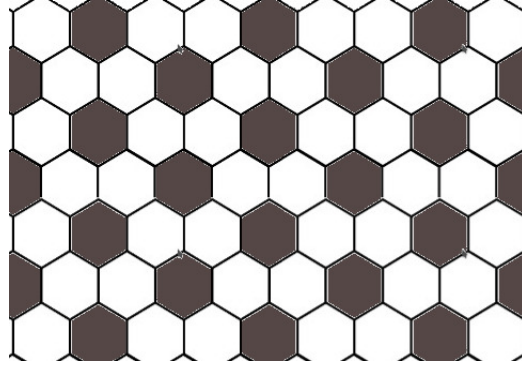


Figure 3.5:  $\rho = 1/3$

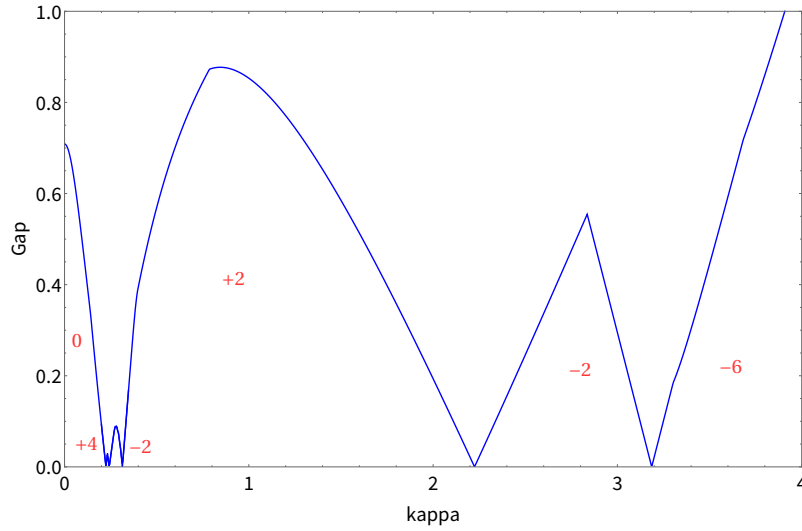


Figure 3.6: Gap as a function of  $\kappa$  for a vortex density  $\rho = \frac{1}{3}$  vortex density. Chern numbers are indicated in red.

It can be seen that our results on plotting the gap as a function of  $\kappa$  agree with the gapped spectrum at  $\kappa = 0$  for other lattices in this family as well.

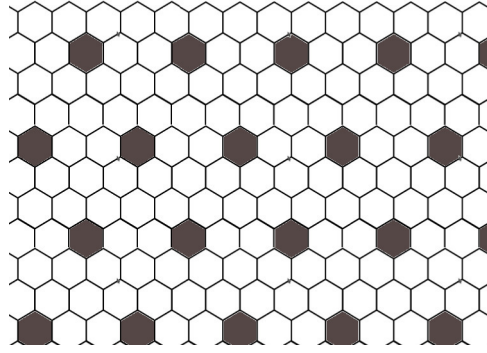


Figure 3.7:  $\rho = 1/9$

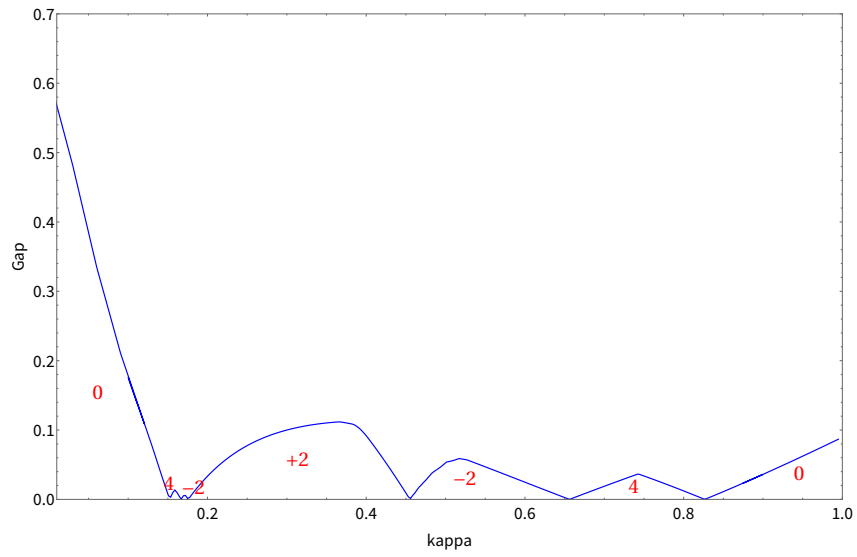


Figure 3.8: Gap as a function of  $\kappa$  for a vortex density  $\rho = \frac{1}{9}$ . Chern numbers are indicated in red.

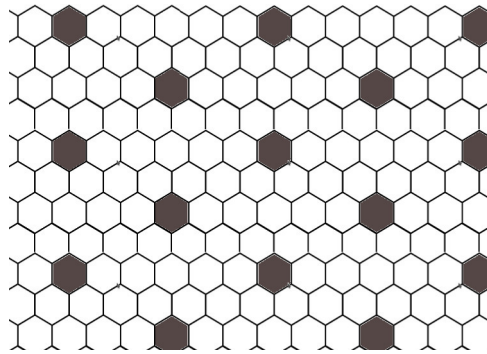


Figure 3.9:  $\rho = 1/12$

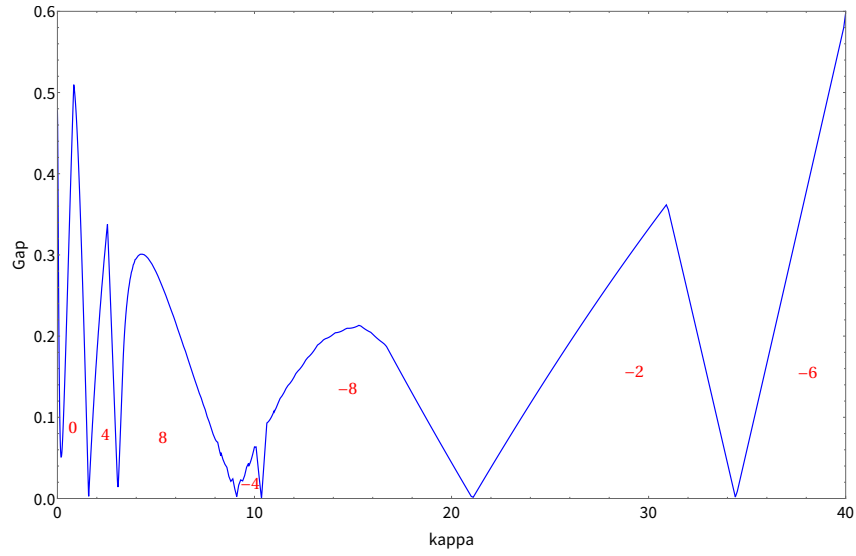


Figure 3.10: Gap as a function of  $\kappa$  for a vortex density  $\rho = \frac{1}{12}$ . Chern numbers are indicated in red.

### 3.6.2 $\rho = \frac{1}{n}$ , where $n$ is not an integral multiple of 3

In this type of vortex configurations, the vortex densities include  $\rho = \frac{1}{4}, \frac{1}{7}, \frac{1}{13}, \dots$  and so on. These vortex configurations have a gapless spectrum at time-reversal invariant point  $\kappa = 0$ . As  $\kappa$  is increased one can observe several gap closings and therefore observe various gapped phases.

For the vortex density of  $\rho = \frac{1}{4}$ , one can observe that there are three points where the gap vanishes giving rise to four gapped phases. The Chern numbers are listed below.

$$v_{1/4}^a = +4, \text{ for } 0 < \kappa < 0.144327, \quad (3.20)$$

$$v_{1/4}^b = 0, \text{ for } 0.144327 < \kappa < 2.46291, \quad (3.21)$$

$$v_{1/4}^c = +4, \text{ for } 2.46291 < \kappa < 2.54644, \quad (3.22)$$

$$v_{1/4}^d = -8, \text{ for } 2.54644 < \kappa. \quad (3.23)$$

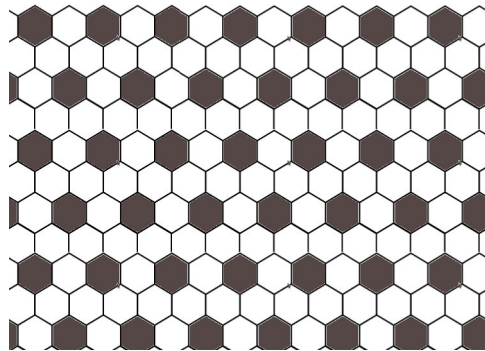


Figure 3.11:  $\rho = 1/4$

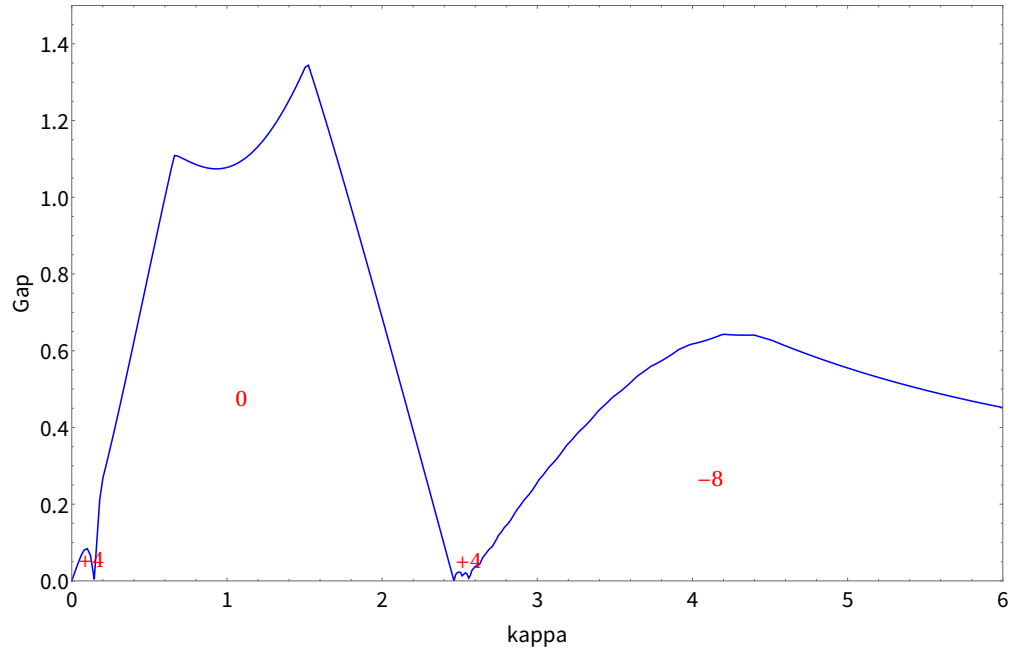


Figure 3.12: Gap as a function of  $\kappa$  for a vortex density  $\rho = \frac{1}{4}$ . Chern numbers are indicated in red.

For the vortex density of  $\rho = \frac{1}{7}$ , one can observe that there are four points where the gap vanishes giving rise to five gapped phases as listed below.

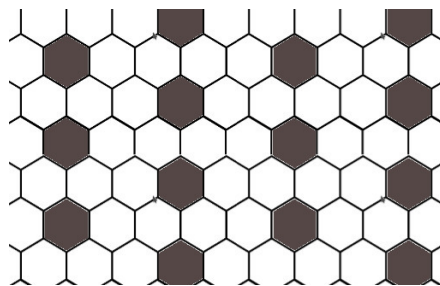


Figure 3.13:  $\rho = 1/7$



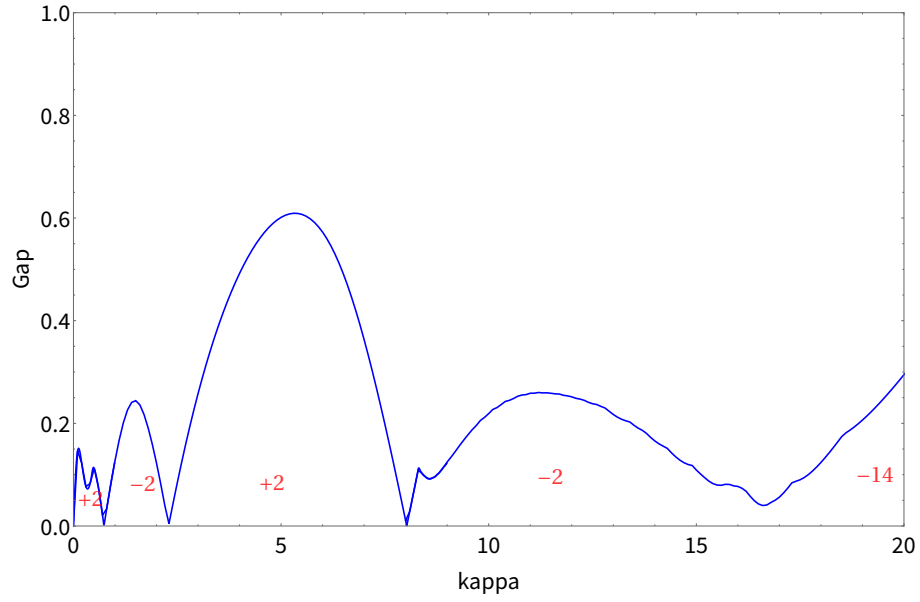


Figure 3.14: Gap as a function of  $\kappa$  for a vortex density  $\rho = \frac{1}{7}$ . Chern numbers are indicated in red.

### 3.7 $\rho = \frac{n-1}{n}$

This family of lattices is a dual to the  $\rho = \frac{1}{n}$  family as we now have white plaquettes in a sea of black plaquettes instead of black plaquettes in white sea for the direct family of lattices. It is characterized by the anti-vortices (absence of vortex - white plaquettes) on top of the vortex-full background (black plaquettes). This type of vortex configurations are close to the vortex-full case in the dilute antivortex limit. They present a rich variety of phases with both odd and even Chern numbers and the presence of various gapless and gapped phases.

For the vortex density of  $\rho = \frac{2}{3}$ , one can observe in figure [3.15] that there are two points where the gap vanishes giving rise to three gapped phases as listed below.

$$v_{2/3}^a = +3, \text{ for } 0 < \kappa < 0.288675, \quad (3.24)$$

$$v_{2/3}^b = -1, \text{ for } 0.288675 < \kappa < 1.1547, \quad (3.25)$$

$$v_{2/3}^c = -2, \text{ for } 1.1547 < \kappa, \quad (3.26)$$

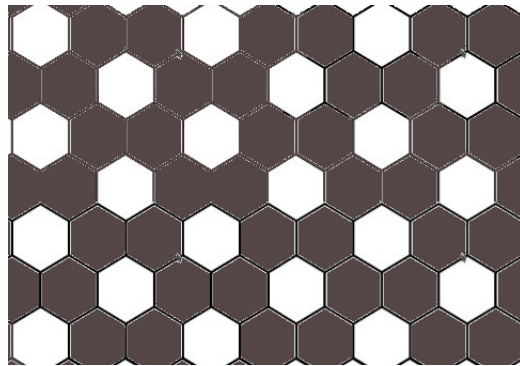


Figure 3.15:  $\rho = 2/3$

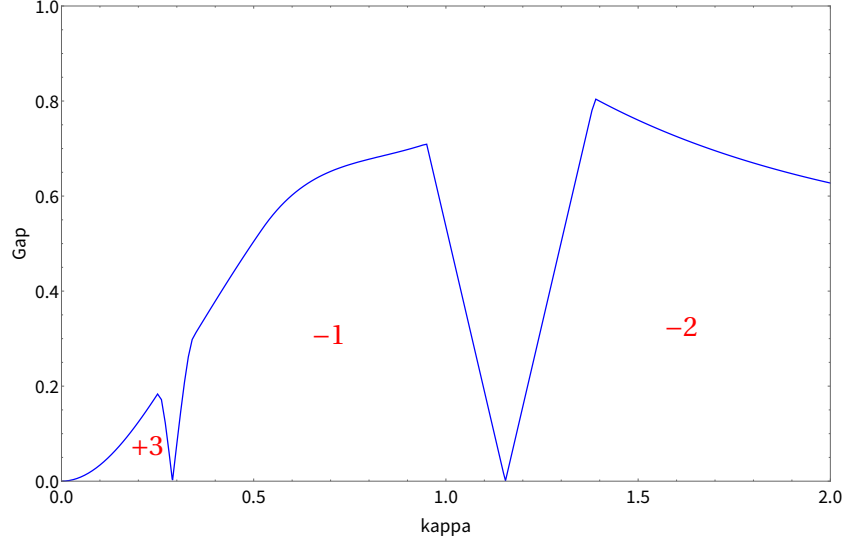


Figure 3.16: Gap as a function of  $\kappa$  for a vortex density  $\rho = \frac{2}{3}$ . Chern numbers are indicated in red.

As we can observe above, this vortex configuration consists of phases having odd and even Chern numbers. Note that these odd Chern numbers are not found in  $\rho = 1/n$  family of vortex lattices. Furthermore, it can be seen that all the configurations with vortex density  $\rho = m/n$  where  $m$  is odd has solely the even Chern numbers. But if  $m$  is even then we can get both odd and even Chern numbers. In the following example of  $\rho = 3/4$ , one can see that the Chern numbers obtained are only even.

For the vortex density of  $\rho = \frac{3}{4}$ , one can observe that there are points in  $\kappa$  space where the gap vanishes and it remains gapless giving rise to the extended gapless phases. These extended gapless phases can not be described by a Chern number. However, there are also some gapped phases as listed below.

$$\text{gapless for } 0 < \kappa < 0.3082, \quad (3.27)$$

$$v_{3/4}^a = +2, \text{ for } 0.3082 < \kappa < 0.3535, \quad (3.28)$$

$$\text{gapless for } 0.3535 < \kappa < 1.0412, \quad (3.29)$$

$$v_{3/4}^b = -2, \text{ for } 1.0412 < \kappa < 1.07809, \quad (3.30)$$

$$\text{gapless for } 1.07809 < \kappa < 1.137117 \quad (3.31)$$

$$v_{3/4}^c = -4, \text{ for } 1.37117 < \kappa, \quad (3.32)$$

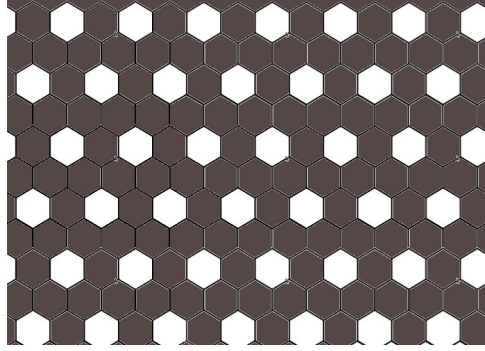


Figure 3.17:  $\rho = 3/4$

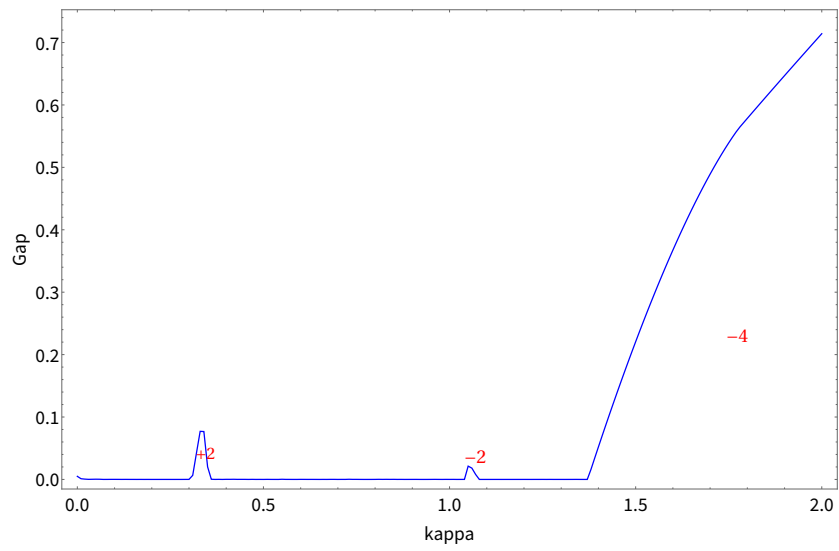


Figure 3.18: Gap as a function of  $\kappa$  for a vortex density  $\rho = \frac{3}{4}$ . Chern numbers are indicated in red.

# Chapter 4

## Table of Chern numbers and observations

### 4.1 $\rho = \frac{1}{n}$

Vortex density →	Vortex free	1/3*	1/4	1/7	1/9*	1/12*	1/13	1/16	1/19	1/21*	1/25
Chern numbers ↓ increasing $\kappa$	1	0	4	2	0	0	2	2	2	0	2
		4	0	-2	4	4	-2	-2	-2	4	-2
		-2	4	2	-2	8	4	4		-2	4
		2	-8	-2	2	-4	0	0		2	0
		-2		-14	-2	-8	4	4		-2	4
		-6			4	-2	-2				-2
					0	-6	2				2
					4		-2				-2
					-2						4
											0
											4
											-2

Figure 4.1: Chern numbers for  $\rho = 1/n$ . Vertical axis has increasing  $\kappa$  value (from top to bottom). When  $n$  is a multiple of 3, it is indicated with a \*. Such lattices have  $\nu = 0$  at  $\kappa = 0$ .

Some observations about the Chern numbers for vortex density  $1/n$ :

- Chern numbers change only by 4, 6, 8 or 12
- When  $n$  is a multiple of 3 then the system is gapped at  $\kappa = 0$  and  $\nu = 0$  at very small  $\kappa$
- All of the listed Chern numbers are even (explained earlier)
- The dilute vortex limit ( $\rho = 1/n$  where  $n \gg 1$ ) is subtle in this family because when the vortex density is very dilute, the system should be gapless with isolated vortices and isolated MZM. One expects a big degenerate subspace at zero energy due to a zero energy state from isolated Majorana mode at each vortex. However, any remaining coupling between them lifts the degeneracy, opens a gap and produces a Chern number. See how  $\rho = 1/25$  is complicated and very different from vortex-free sector  $\rho = 0$ . A notable difference is that the systems at  $\rho = 1/n$  for very large  $n$  has only the even Chern numbers, whereas  $\rho = 0$  has  $\nu = 1$ .

## 4.2 $\rho = \frac{n-1}{n}$

Vortex density $\rightarrow$ Chern numbers $\downarrow$ increasing $\kappa$	1 (Vortex full)	2/3	3/4	6/7	8/9	11/12*	12/13	15/16	18/19	20/21	24/25	26/27	27/28	30/31	36/37	38/39	42/43
	2	3	-	2	0	0	1	-	1	0	1	0	-	1	1	0	1
	-2	-1	2	1	2	-	2	2	2	2	2	2	2	2	2	2	2
		-2	-	-2	1	2	-1	-	1	-1	1	-1	-	-1	1	1	-1
			-2	-5	-2	-	-2	-2	-2	-2	-2	-2	-2	-2	-2	-2	-2
			-	1		-2		-					-				
			-4			-		0					-4				
						0											

Figure 4.2: Chern numbers for  $\rho = (n-1)/n$ . Vertical axis has increasing  $\kappa$  value (from top to bottom). When  $n$  is a multiple of 12, it is indicated with a \*. The flux in the triangles (joining vortex sites) is  $\phi$ . Red indicates  $\phi = 0$ , green indicates  $\phi = \pi$ , blue indicates  $\phi = -\pi/2$ . Extended gapless phases indicated by the symbol -.

- Odd Chern numbers appear along with the even Chern numbers
- When  $n$  is even, the parity of  $\nu$  is conserved when  $\kappa$  varies. If  $n$  is odd, the parity may vary with  $\kappa$
- When  $n$  is even, an extended gapless phases occur (indicated by the symbol -) in the table
- When  $n$  is a multiple of 3, small  $\kappa$  phase has  $\nu = 0$  except for the 2/3 case (we have no explanation for that yet)
- When  $n$  is a multiple of 12 then the system is gapped at  $\kappa = 0$  at very small  $\kappa$ . This gap opening can be explained using an argument similar to [4] based on coupling of Dirac cones. The vortex-full lattice has a gapless band structure at  $\kappa = 0$ , due to the presence of four Dirac cones given earlier. The triangular antivortex superlattice from  $\rho = 11/12$  lattice on top of the vortex-full background creates a perturbing potential (compared to the vortex-full case) which has the same periodicity as the antivortex superlattice. The reciprocal lattice vectors of the  $\rho = 11/12$  lattice can give a linear combinations equal to  $\mathbf{K}_{f1} - \mathbf{K}_{f2}$ ,  $\mathbf{K}_{f1} -$

$\mathbf{K}_{f3}$ ,  $\mathbf{K}_{f1} - \mathbf{K}_{f4}$  and  $\mathbf{K}_{f3} - \mathbf{K}_{f4}$  thereby coupling the pairs of Dirac cones and resulting into opening of the gap (We need not check for the  $\mathbf{K}_{f2} - \mathbf{K}_{f3}$  and  $\mathbf{K}_{f2} - \mathbf{K}_{f4}$  as it is redundant due to the symmetries).

- For the dual lattices, the dilute antivortex limit is more obvious. When  $\rho = (n - 1)/n$  with large  $n$ , the main phases are  $\nu = 2$  before  $\kappa = 0.5$  and  $\nu = -2$  after, as for the vortex-full case  $\rho = 1$ .

### 4.3 Vortex densities of $\rho = 4/7$ , $\rho = 2/7$ , $\rho = 4/9$ , $\rho = 6/9$ in search for the Chern numbers $\nu = \pm 7$

It can be seen from the tables of Chern numbers that we have 14 distinct types of Chern numbers but the Chern number of either  $\nu = \pm 7$  or 7 and 9 is still missing. The Chern number from these classes would complete the 16-fold way in the Kitaev model. Although the triangular vortex lattices studied here do not show  $\nu = 7 \pmod{16}$ , they hint to the potential lattices where the missing Chern number could be found. It is clear that, to obtain the odd Chern number, we need to explore the lattices where the vortex density is  $\rho = \frac{\text{even}}{\text{odd}}$ . It can be seen that the higher Chern numbers like 3 and  $-5$  are found for the dense antivortex lattices. As antivortex density is diluted (close to the vortex-full) we get only the  $\nu = 0, \pm 1, \pm 2$ . Therefore, relatively denser antivortex lattices with densities  $\rho = 4/7$ ,  $\rho = 2/7$ ,  $\rho = 4/9$ ,  $\rho = 6/9$  can be explored to check for the missing Chern number.

We studied the triangular vortex lattices of these vortex densities  $\rho = 4/7$ ,  $\rho = 2/7$ ,  $\rho = 4/9$ ,  $\rho = 6/9$  for all the possible configurations and found that the missing Chern number does not exist in these lattices. It is possible that the missing Chern number is found in other vortex lattices like striped lattices of the same vortex density as we had explored.



# Chapter 5

## Effective Majorana model for $\rho = \frac{1}{n}$ lattices

Dilute vortex lattices where  $\rho = \frac{1}{n}$  with  $n \gg 1$  can be studied and the observations regarding Chern numbers can be explained using the effective models in Majorana.

### 5.1 A vortex pair interaction

Adding a single vortex to a chiral p-wave superconductors, the vortex cores hosts a localised zero energy state called as Majorana zero mode in the vortex core [10]. This idea is related to the Caroli-de Gennes-Matricon states [20] in the vortex cores of usual superconductors and Abrikosov vortex lattice in topological superconductors [21]. As we have a finite system with periodic boundary conditions we cannot have a single vortex in the system, vortices always come in pairs. So to begin, we can study 2-vortex problem. We need to understand the behavior of vortex-vortex interaction in our model. The simplest case one can study is the interaction between a pair of vortices separated by a distance  $d$ . This is already studied in ref. [22], [2], [26]. It is known that a vortex has a Majorana zero mode (a mode in the vortex core with  $E = 0$ ) bound to it. When a pair of vortex are at a distance  $d$  on the background of a vortex-free lattice, the hybridization of the Majorana zero modes occur leading to splitting of the energy levels near zero energy.

The energy difference between the levels closest to zero  $E_1 - (-E_1) = 2E_1$  is called the energy splitting. The absolute magnitude of the energy splitting oscillates but increases overall as the vortices are placed closer. Thus energy splitting is a function of inter-vortex distance  $d$ . It is also a

function of time-reversal breaking  $\kappa$  term. This is shown in the figure [5.1].

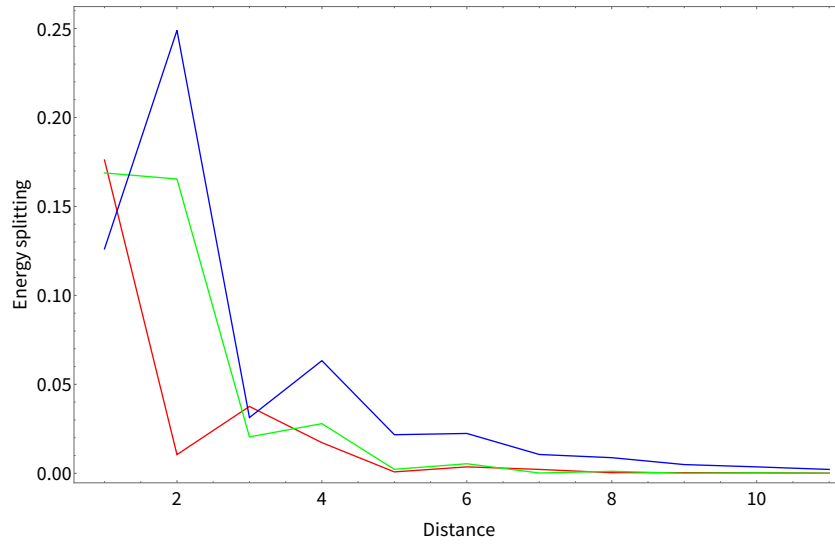


Figure 5.1: The absolute value of energy splitting as a function of distance between a pair of vortices, Red curve indicates  $\kappa = 0.1$ , green curve indicates  $\kappa = 0.4$ , blue curve indicates  $\kappa = 0.7$ .

The absolute magnitude of energy splitting also depends upon  $\kappa$ . It can be seen from figure [5.2] that as  $\kappa$  increases the energy splitting increases as well, reflecting stronger vortex-vortex interaction at higher  $\kappa$ .

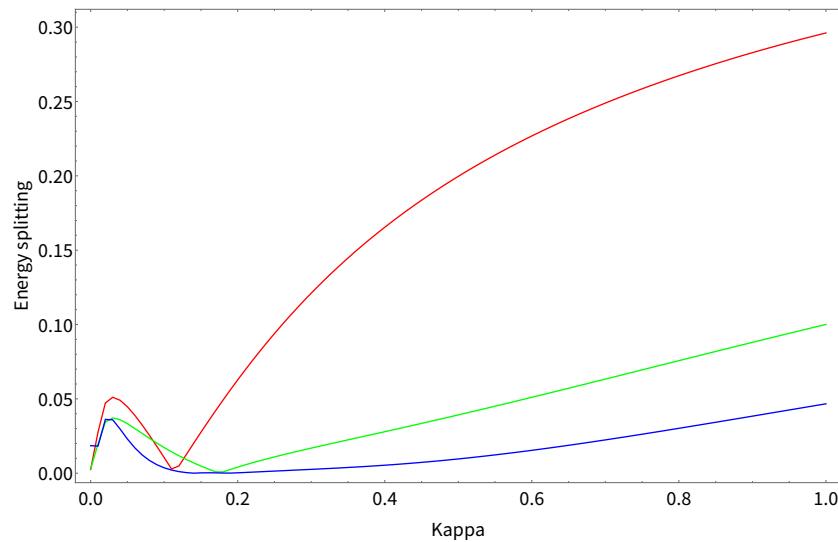


Figure 5.2: The absolute value of energy splitting as a function of  $\kappa$  for different distances. Red curve indicates  $d = 2$ , green curve indicates  $d = 4$ , blue curve indicates  $d = 6$ .

The tunneling amplitude of a pair of Majorana modes in the  $p_x + ip_y$  superconductors was already studied [6]. We therefore expect the exponential and oscillatory decrease of tunneling amplitude with respect to distance according to the equation

$$2t_1 \sim \Delta_b \cos(k_F d) \exp(-d/\xi) \quad (5.1)$$

where  $\Delta_b$  is the background gap,  $\xi = v_F/\Delta_d$  is the coherence length,  $k_F$  is the distance between the center of BZ and the Fermi surface,  $\hbar = 1$  and  $a = 1$  and the Fermi velocity  $v_F \sim W_b$  where  $W_b$  is the bandwidth of the background. This shows how the Majorana modes are localised in the vortex cores and the tunneling between the pair of MZM once they are brought closer. The sign of the tunneling amplitude is decided by  $t_1 = (-1)^{Pd} E_1$  where  $Pd$  is the physical fermionic parity which exists due to the transformation of spin Hamiltonian into Majorana Hamiltonian. The sign of the tunneling amplitude has implications on the anyonic excitations. Following the fusion rule  $\sigma \times \sigma = 1 + \varepsilon$ ; if  $t_1 < 0$ , then the system favours the fermionic excitation ( $\varepsilon$ ) and the trivial excitation (1) if  $t_1 > 0$ .

Our study as shown in figure [5.1] confirms this trend qualitatively.

## 5.2 Formation of vortex bands

Now imagine a triangular lattice of vortices with the tunneling turned off. This means that the system has a huge degeneracy (due to many MZM at exactly zero energy). Then if the tunneling is turned on (i.e. allowing the Majorana fermions to tunnel from one vortex to another), it gives rise to a collective state or a band. These bands are formed due to the vortex-vortex interactions, so they will be called the "vortex bands".

Following the idea from ref [2], [26], the Chern numbers can be found separately for the low-energy vortex bands (due to the vortex superlattice) and for the high energy fermion bands (due to the vortex-free background). The total Chern number  $\nu$  is then

$$\nu = \nu_f + \nu_v \quad (5.2)$$

where  $\nu_f = 1$  for the fermion bands of the vortex-free sector and  $\nu_v$  is the Chern number for the vortex bands. This assumption is true only if the gap between the low energy vortex bands and high energy fermion bands is large enough. If the vortex bands touch the fermion bands then one

simply cannot use this assumption.

This assumption is helpful because now we need to focus only on the vortex bands. As  $\nu_f = 1$  is already known, the Chern numbers from vortex bands decide the total Chern number. Therefore we need a model to describe the physics of low energy vortex bands, more precisely a Hamiltonian for the vortex superlattice from which the Chern numbers for the vortex bands can be obtained.

### 5.3 Hamiltonian for the effective model

For a triangular lattice of vortices (on top of the background vortex-free lattice), an effective tight binding model of Majoranas hopping on the triangular lattice can be thought of. The Hamiltonian for this can be written as

$$H = \sum_{i,j} t_{ij} \gamma_i \gamma_j \tag{5.3}$$

Here, each vortex has a Majorana operator  $\gamma_i$  associated with it,  $t_{ij} \in \mathbb{R}$  and the flux through each triangle can only be  $\pm\pi/2$ . The Majoranas hop on the triangular superlattice as shown in 5.3. The vortex superlattice forms the low energy vortex bands in addition to the high energy fermion bands of the vortex-free background. The Chern numbers for the vortex bands  $\nu_v$  can be found using this Hamiltonian.

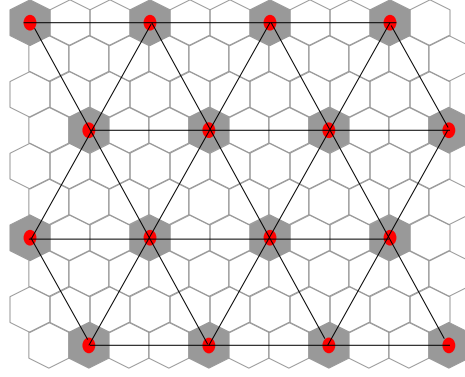


Figure 5.3: The triangular vortex lattice for  $\rho = 1/9$ . Vortices are shown in grey and Majorana modes in each vortex by red dots. The triangular vortex superlattice is shown.

In the earlier study [2], the effective model consists of nearest  $t_1$  and next -nearest  $t_{\sqrt{3}}$  hopping amplitudes. The Majorana Hamiltonian is  $H(\mathbf{k}) = \vec{m}(\mathbf{k}) \cdot \vec{\sigma}$  where  $\mathbf{a}_1$ ,  $\mathbf{a}_2$  are defined as earlier,  $\mathbf{a}_3 = \mathbf{a}_1 - \mathbf{a}_2$  and

$$m_x(k) = -2t_1 \sin(\mathbf{k} \cdot \mathbf{a}_3) + 2t_{\sqrt{3}} \sin(\mathbf{k} \cdot [\mathbf{a}_1 + \mathbf{a}_2]), \quad (5.4)$$

$$m_y(k) = 2t_1 \sin(\mathbf{k} \cdot \mathbf{a}_2) + 2t_{\sqrt{3}} \cos(\mathbf{k} \cdot [\mathbf{a}_1 + \mathbf{a}_3]), \quad (5.5)$$

$$m_z(k) = 2t_1 \sin(\mathbf{k} \cdot \mathbf{a}_1) - 2t_{\sqrt{3}} \sin(\mathbf{k} \cdot [\mathbf{a}_3 - \mathbf{a}_2]), \quad (5.6)$$

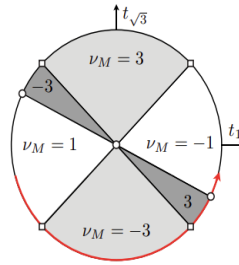


Figure 5.4: Phase diagram found by considering  $t_1$  and  $t_{\sqrt{3}}$  by Lahtinen et al.[2] Here,  $\nu_M$  is the same as  $\nu_\nu$ .

If only  $t_1$  is non-zero, i.e. when  $t_1$  dominates, it is a single copy of the triangular lattice. This

is the case of triangular lattice with  $\pi/2$  flux per triangle. It is well studied in what is known as the Claro-Wannier butterfly [9]. For  $\pi/2$  flux per triangle in triangular lattice the spectrum is gapped having two symmetric bands separated by a band gap. From the Claro-Wannier butterfly, one expects the Chern number to be  $\pm 1$ . Note the difference that the concerned bands here are of real fermions instead of complex fermions. When only the  $t_{\sqrt{3}}$  is non-zero then we have  $\nu_v = \pm 3$ . This is because when  $t_{\sqrt{3}}$  dominates there are three decoupled copies of triangular lattices each giving a Chern number of  $\pm 1$  which combines to give  $\nu_v = \pm 3$ .

Therefore, the total Chern number is  $\nu = 0, \pm 2$  or  $4$  (using  $\nu = \nu_f + \nu_v$ ).

## 5.4 Validity of the effective model

Effective model is valid only when the background gap (which appears due to the vortex-free or the vortex-full sector in the background) is larger than the bandwidth of the vortex bands appearing near zero energy. This means that the vortex bands have to be well-separated from the background bands. For the vortex-free case the spectrum is gapless at  $\kappa = 0$  so the effective model fails at  $\kappa = 0$ . It could also fail at  $\kappa = 0$  for  $\rho = 1/n$  vortex lattices where  $n$  is an integral multiple of 3. Although there exists a gapped phase at  $\kappa = 0$  as seen in the microscopic model, this gap need not be equal to the gap due to Majorana modes from the vortex superlattice. Therefore, the effective model would fail at  $\kappa = 0$  for this family of vortex density as well.

At  $\kappa > \kappa_h$  and at  $\kappa < \kappa_l$ , the energy gap between the vortex bands and background band vanishes as the vortex bands become comparable to the bulk bands. Therefore the effective model is valid only in a finite range of  $\kappa$ ; from  $\kappa_l$  to  $\kappa_h$  where  $0 \leq \kappa_l < \kappa < \kappa_h$ .

The range of validity is different for different lattices characterized by inter-vortex distance  $d$ . The reason is that the vortex band gap  $2t_1(\kappa, d)$  is a function of inter-vortex distance  $d$ .  $2t_1(\kappa, d)$  is an estimate of the vortex bandwidth and  $\Delta_b(\kappa)$  is the size of the gap (for the vortex-free background). A necessary condition for the validity of the model is that the vortex bands should be well separated from the bulk bands. This condition is satisfied when the inequality given by the following equation is true.

$$2t_1(\kappa, d) \ll \Delta_b(\kappa) \tag{5.7}$$

So the inter-vortex distance which in turn determines the vortex density of the lattice (using  $d = \sqrt{n}$ ) gives the range of  $\kappa$  where the effective model is valid.

We already know the equation

$$2t_1 \sim \Delta_b \cos(k_F d) \exp(-d/\xi) \sim \Delta_b \exp(-d/\xi) \quad (5.8)$$

And noting the relations  $k_F \xi = E_F/\Delta \approx (W_b/2)/\Delta_b$  and therefore  $\xi/2 \sim W_b/\Delta_b$ , the validity criterion is set by the idea that the coherence length should be very small compared to the inter-vortex distance for the corresponding vortex lattice. This can be set as

$$\xi < d \text{ or } d/2 \quad (5.9)$$

The gap for the vortex-free background is already known,  $\Delta_b = \min(2, 6\sqrt{3})$ . The bandwidth is found to be  $W_b = \max(6, 6\sqrt{3})$  and  $v_F \sim W_b/3$ . If  $\xi = d$  then

$$\kappa_l \sim \frac{1}{3\sqrt{3}d} \quad (5.10)$$

$$\kappa_h \sim \frac{d}{\sqrt{3}} \quad (5.11)$$

Now taking a vortex lattice with  $d = 4$ , we see that  $\kappa_l \sim 0.05$  and  $\kappa_h \sim 2$ , for  $\xi = d$ . Now another criterion could be  $\xi = d/2$  then  $\kappa_l \sim 0.1$  and  $\kappa_h \sim 1$ , for  $\xi = d/2$ .

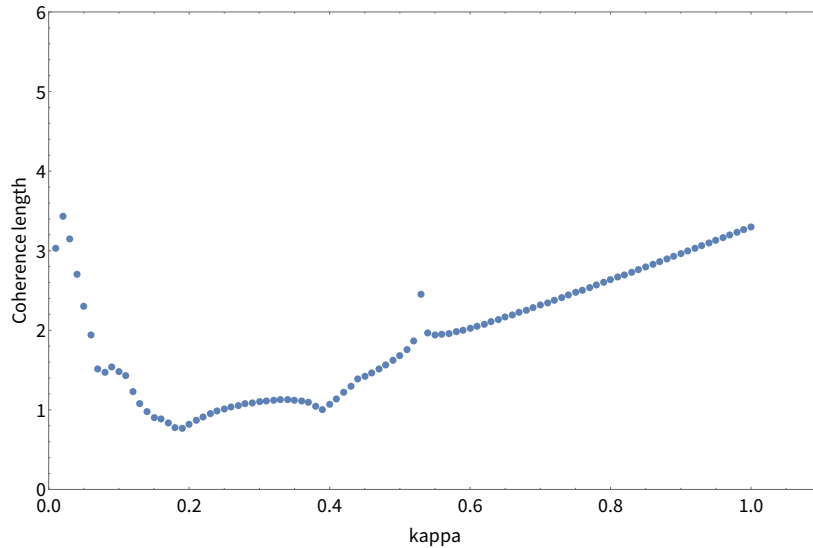


Figure 5.5: Coherence length (in the units  $a = |\mathbf{a}_1| = |\mathbf{a}_2| = 1$ ) as a function of  $\kappa$

## 5.5 Obtaining hopping parameters from microscopic model

The effective model fails at  $\kappa > \kappa_h$ . Therefore the higher Chern numbers found in the range  $\kappa > \kappa_h$  cannot be explained using this effective model. For the range of  $\kappa$  where the effective model is valid, the only hopping parameters needed are  $t_1$  and  $t_{\sqrt{3}}$ . The longer hopping terms can be neglected as compared to  $t_1$  and  $t_{\sqrt{3}}$  because the longer terms are not significant in the region of validity of the effective model.  $t_1$  and  $t_{\sqrt{3}}$  can be extracted from the microscopic model involving the use of a vortex-free patch with either only 2 or 3 or 4 vortices. The main step in this involves calculating the spectrum for the given configuration of vortices from microscopics.

For the 2-vortex case, the energy splitting  $\varepsilon(d)$  is calculated when the vortices are kept at a distance  $d$  corresponding to either the nearest-neighbor vortex distance in the triangular lattice (if  $t_1$ ) or the next-nearest neighbor (if  $t_{\sqrt{3}}$ ) distance. For example, for the 1/4 vortex lattice, the vortices are kept at a distance  $d = 2$  and the energy of the first level (closest to zero) is calculated from the spectrum of microscopic Hamiltonian. This would give  $t_1$  after multiplying by proper parity as

$$t_d = (-1)^{P_d} \varepsilon_d \quad (5.12)$$

where  $P_d$  is the physical fermionic parity which exists due to the transformation of spin Hamiltonian into Majorana Hamiltonian. Similarly if vortices are kept at a distance  $d = 2\sqrt{3}$ , following the same procedure would give us  $t_{\sqrt{3}}$ .

The 2-vortex case does not have a triangle of vortices. Therefore, there is no concept of flux within a triangle for 2-vortex case. Moreover, we claim that adding more vortices to the lattice would make the hopping parameter more accurate. That is why we study 3-vortex and 4-vortex case.

For the 3-vortex case, we choose 4 vortices including an equilateral triangle of side  $d$  and a fourth vortex at a much farther distance from this triangle. There are 4 vortices here because we work on a finite system with periodic boundary conditions and therefore only an even number of vortices is possible. This arrangement gives us four energy levels  $\pm E(d, \kappa)$  and two zeroes as seen in the spectrum of microscopic model. It is obvious that there is one zero for the isolated vortex. The second zero comes from the structure of the Hamiltonian describing the 3-vortex problem. As it is a Hamiltonian for Majoranas, it has a  $E$  to  $-E$  symmetry but here it is  $3 \times 3$  and therefore only 3 energy levels. There must at least be one at zero energy and the two others are  $E$  and  $-E$ , therefore giving four energy levels as  $\pm E(d, \kappa)$  and two zeroes. To relate these energy levels with



the hopping parameters we need to write the Majorana Hamiltonian for the vortex-triangle and then diagonalize it.

$$H_{3v} = i \begin{bmatrix} 0 & -t_1 & -t_1 \\ t_1 & 0 & -t_1 \\ t_1 & t_1 & 0 \end{bmatrix} \quad (5.13)$$

The hopping amplitude are then found to be  $t_1 = E(d, \kappa)/\sqrt{3}$ . The same procedure can be repeated to find  $t_{\sqrt{3}}$ .

The 4-vortex case contains a rhombus of vortices where the energy levels are  $\pm E_1(d, \kappa)$  and  $\pm E_2(d, \kappa)$ . To relate these energy levels with the hopping parameters we need to write the Majorana Hamiltonian and then diagonalize it. The fluxes in the triangles ( $\pi/2$  for  $d = 1$  and  $-\pi/2$  for  $d = \sqrt{3}$ ) decide the gauge signs of the hopping parameters in the following Majorana Hamiltonian.

$$H_{4v} = i \begin{bmatrix} 0 & -t_1 & -t_1 & t_{\sqrt{3}} \\ t_1 & 0 & -t_1 & t_1 \\ t_1 & t_1 & 0 & -t_1 \\ t_{\sqrt{3}} & -t_1 & t_1 & 0 \end{bmatrix} \quad (5.14)$$

The eigenvalues are

$$E = \pm \frac{\sqrt{5t_1^2 + t_{\sqrt{3}}^2 \pm (t_1 + t_{\sqrt{3}}) \sqrt{9t_1^2 - 2t_1 t_{\sqrt{3}} + t_{\sqrt{3}}^2}}}{\sqrt{2}} \quad (5.15)$$

The hopping amplitudes  $t_1$  and  $t_{\sqrt{3}}$  can then be found by simplifying and solving the above equations.

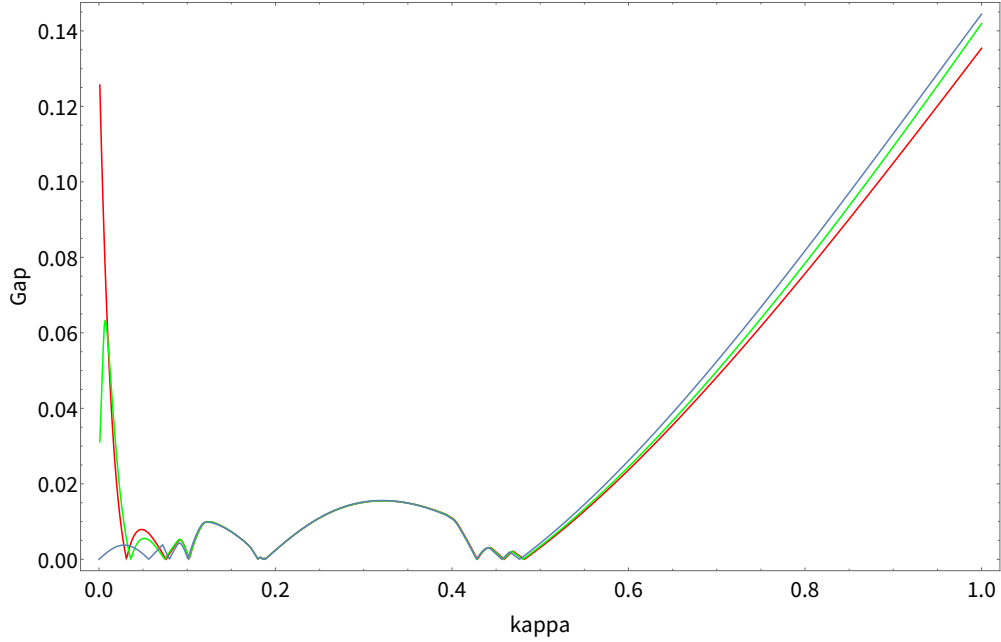


Figure 5.6: Gap vs kappa for  $1/25$  vortex density. Microscopic curve is in blue, the curve from the effective model for 2-vortex case is in red, the curve from the effective model for 3-vortex case is in green.

It can be seen from figure 5.6 that the behaviour for the gap as a function of  $\kappa$  from the effective model matches with the microscopics to a good accuracy. Using equations 5.10 and 5.11, we can find the validity range for the  $\rho = 1/25$  lattice. It turns out that  $\kappa_l \sim 0.04$  and  $\kappa_h \sim 2$ . The plot in figure 5.6 in the range  $0.04 < \kappa < 1$  indeed shows a good match between two models as expected. It also demonstrates the improved accuracy for the 3-vortex case over 2-vortex case as expected.

## Chapter 6

# Effective Majorana model for $\rho = \frac{n-1}{n}$ lattices

Similar to the earlier study of  $\rho = \frac{1}{n}$  lattices, the antivortex lattices where  $\rho = \frac{n-1}{n}$  can be studied and the observations regarding Chern numbers can be explained using the effective models. The effective models here would involve spinless  $p_x + ip_y$  superconductivity on a triangular lattice.

The vortex-full background has  $\nu_f = \pm 2$ . Due to this, the creation of antivortex (white plaquette) in the system would bind to it a single complex fermion mode at energy  $\varepsilon$ ; or equivalently, it binds a pair of MZM that hybridize via a term proportional to  $\varepsilon$  and therefore are no longer at energy 0 but  $\pm\varepsilon$ . This is different than a single MZM bound to the vortex near the vortex-free case as seen earlier. As these two real Majorana modes are equivalent to one complex fermionic mode, a single vortex now carries a complex fermionic mode. We want to build a nearest-neighbor hopping model on the triangular lattice for these complex modes with the condition that time-reversal symmetry is broken. We know the flux in each triangle which could help us break the TRS. However when this flux is 0 or  $\pi$ , it does not break the TRS by itself. That's why we take a BdG model with  $p_x + ip_y$  superconductivity to describe our model. See figure 6.1. The fluxes in the triangles joining the anti-vortices determine the unit cell. These fluxes are found out to be

$$\phi_n = (n-1)\pi/2[2\pi] \tag{6.1}$$

Depending upon the flux in the triangles, there are three sub-families of lattices in the  $\rho = \frac{n-1}{n}$

family of lattices. The flux in the triangles can only be  $0$ ,  $\pi$  and  $-\pi/2$  which correspond to the red, green and blue family as shown in the table 4.2. Here  $0$  and  $\pi$  fluxes do not break the TRS but  $-\pi/2$  does.

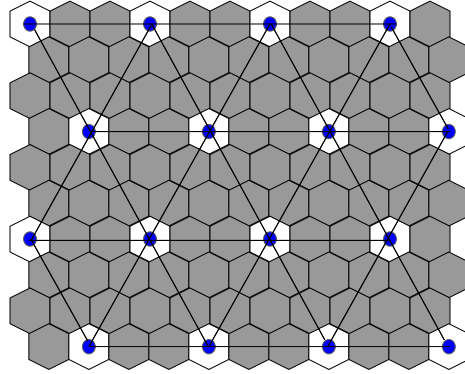


Figure 6.1: The triangular antivortex lattice for  $\rho = 8/9$ . Anti-vortices are shown in white and complex fermion modes (two Majorana modes) in each vortex by blue dots. The triangular vortex superlattice is shown.

## 6.1 $\rho = \frac{n-1}{n}$ lattices where $n-1$ is an even number

These vortex lattices can have flux per triangle to be either  $\phi = 0$  or  $\phi = \pi$ .

### 6.1.1 $\phi = 0$

This family of lattices has the vortex densities of  $\frac{8}{9}$ ,  $\frac{12}{13}$ ,  $\frac{20}{21}$ ..... As there is no flux in the triangles, the unit cell is not extended as the unit cell for Hamiltonian is equal to the geometrical unit cell. The Bravais lattice vectors are  $\mathbf{a}_3$  and  $\mathbf{a}_1$  where  $\mathbf{a}_1 = (1/2, \sqrt{3}/2)$ ,  $\mathbf{a}_2 = (1/2, -\sqrt{3}/2)$  and  $\mathbf{a}_3 = \mathbf{a}_1 - \mathbf{a}_2$ .

The Bogoliubov-de Gennes (BdG) Hamiltonian for this family is a 2x2 matrix given as

$$H(\mathbf{k}) = \begin{bmatrix} H_0(\mathbf{k}) & \Delta(\mathbf{k}) \\ \Delta(\mathbf{k})^* & -H_0(-\mathbf{k}) \end{bmatrix} \quad (6.2)$$

where the Nambu spinor is taken as  $(c_{\mathbf{k}}, c_{-\mathbf{k}}^\dagger)^T$ . Here the single particle Hamiltonian is

$$H_0(\mathbf{k}) = \varepsilon - 2t \sum_j \cos \mathbf{k} \cdot \mathbf{a}_j \quad (6.3)$$

where  $\varepsilon = -\mu$  is the on-site energy and  $t$  is the nearest neighbour hopping amplitude. The superconducting pairing term is

$$\Delta(\mathbf{k}) = 2i\Delta \sum_j (\mathbf{u}_x + i\mathbf{u}_y) \cdot \mathbf{a}_j \sin \mathbf{k} \cdot \mathbf{a}_j \quad (6.4)$$

where  $\Delta > 0$ . When  $\Delta = 0$ , the BdG Hamiltonian obeys TRS. However if  $\Delta \neq 0$  then TRS is not present and non-zero Chern numbers are possible. The Hamiltonian has the inversion symmetry

$$\tau_z H(-\mathbf{k}) \tau_z = H(\mathbf{k}) \quad (6.5)$$

where  $\tau_z$  is the Pauli matrix in Nambu space. This means that the spectrum is identical upon the change  $\mathbf{k} \rightarrow -\mathbf{k}$ . Therefore, the gap closings seem to appear in pairs. However, there are four special points in BZ,  $\Gamma = (0,0)$ ,  $X = (1/2, 0)$ ,  $Y = (0, 1/2)$  and  $M = (1/2, 1/2)$  that are their own image under inversion as  $\mathbf{k} = -\mathbf{k} \bmod \mathbf{G}$ . At these points, the gap can close alone (no pairs of gap closing). This is because of the absence of the extra symmetry  $\varepsilon(\mathbf{k} + \mathbf{A}_2^*/2) = \varepsilon(\mathbf{k})$  that we had earlier. So the change in Chern number can be odd or even in this case.

The Chern number can again be found using the equation  $\nu = \nu_f + \nu_v$ . Here, the background high-energy fermion bands are those of vortex-full sector with the Chern number  $\nu_f = \pm 2$  depending on  $\kappa > 0.5$  or  $\kappa < 0.5$ . We can find  $\nu_v$  from the 2x2 BdG Hamiltonian. It is found that  $\nu_v = 0, \pm 1, \pm 2$ , see figure 6.1.1. Therefore the total Chern number can be as follows

$$\nu = 0, 1, 2, 3, 4 \quad \text{when } \kappa < 0.5 \text{ or } \nu_f = 2 \quad (6.6)$$

$$\nu = 0, -1, -2, -3, -4 \quad \text{when } \kappa > 0.5 \text{ or } \nu_f = -2 \quad (6.7)$$

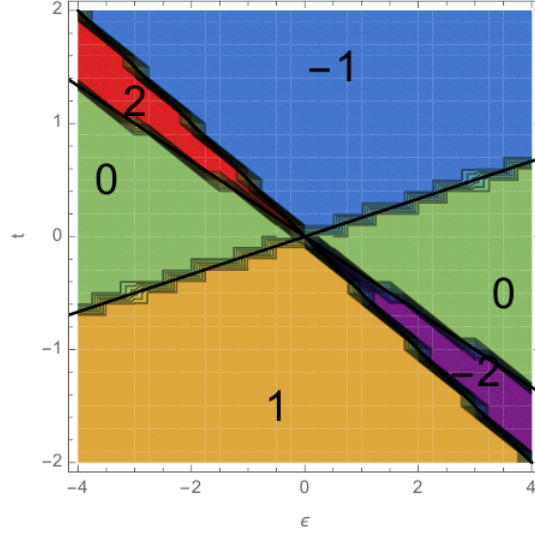


Figure 6.2: Vortex Chern numbers  $v_v$  as a function of  $\epsilon$  and  $t$  when  $\Delta = 1$  obtained from the effective model described in 6.1.1.

### 6.1.2 $\phi = \pi$

This family of vortex lattices have vortex densities of  $2/3, 6/7, 18/19, \dots$ . It can be described by the effective model for  $\phi = 0$  case, taking ' $t$ ' to be negative corresponding to  $\pi$  flux in the triangle.

One can expect that for the dilute lattices, for large  $\kappa$ , the tunneling  $t$  and the pairing term  $\Delta$  becomes negligible as compared to  $\epsilon$  and the vortex bands correspond to a trivial "insulator" i.e.  $v_v = 0$ . Therefore,  $v_v = 0, v_f = -2$  and  $v = -2$ . A trend can be observed that the positive Chern numbers are obtained for  $\kappa < 0.5$  and the negative Chern numbers for  $\kappa > 0.5$

## 6.2 $\rho = \frac{n-1}{n}$ lattices where $n-1$ is odd

For this family, we can not yet write the correct effective model. However we are trying to explain the extended gapless phases by giving the argument about the inversion symmetry.

# Chapter 7

## Conclusion

This thesis has explored the triangular vortex lattices in the Kitaev model in the presence of the time-reversal breaking  $\kappa$  term. We characterized different phases for triangular vortex lattices upon varying  $\kappa$ . The table of Chern numbers gives a good reference to know the types of vortex lattices where a particular topological order could be found.

The 16-fold way classification of the phases in the Kitaev model is almost complete except classes belonging of the type  $\nu = \pm 7$  or  $\nu = 7$  and  $\nu = 9$ . These Chern numbers could be found in other types of vortex lattices (striped lattices, for example) than triangular.

We derived an important result for arbitrary periodic vortex lattices (not restricted to triangular) where odd number of vortices in the geometrical unit cell give only the even Chern numbers. Therefore such vortex lattices provide us with abelian anyons and different topological orders associated with them.

The effective models in Majorana fermions successfully describe the Chern numbers and the behaviour of the gap vs  $\kappa$  upto a range of validity. We have managed to find a few different methods to set the validity range for the effective models and obtained better ways to compute the effective parameters.

We have achieved to find a new approach to build the effective model for the triangular antivortex lattices using  $p_x + ip_y$  superconductivity on a triangular lattice. This could be a useful way to study other types of antivortex lattices in Kitaev model and maybe useful in exploring other

systems with the presence of anti-vortices and even Chern number.



# Bibliography

- [1] A. Kitaev, “Anyons in an exactly solved model and beyond,” *Ann. Phys.* 30021, 2 (2006).
- [2] V. Lahtinen, A.W.W. Ludwig, J.K. Pachos and S. Trebst, “Topological liquid nucleation induced by vortex-vortex interactions in Kitaev’s honeycomb model,” *Phys. Rev. B* 86, 075115 (2012).
- [3] F. Zschocke and M. Vojta, “Physical states and finite-size effects in Kitaev’s honeycomb model: Bond disorder, spin excitations, and NMR line shape,” *Phys. Rev. B* 92, 014403 (2015).
- [4] M. Kamfor, S. Dusuel, K.P. Schmidt, and J. Vidal, “Fate of Dirac points in a vortex superlattice,” *Phys. Rev. B* 84, 153404 (2011).
- [5] V. Lahtinen, J. K. Pachos, “Topological phase transitions driven by gauge fields in an exactly solvable model” *Phys. Rev. B* 81, 245132 (2010).
- [6] M. Cheng, R. M. Lutchyn, V. Galitski, and S. Das Sarma, “Splitting of Majorana-Fermion Modes due to Intervortex Tunneling in a  $px+ipy$  Superconductor,” *Phys. Rev. Lett.* 103, 107001 (2009).
- [7] A. P. Schnyder, S. Ryu, A. Furusaki, and A. W. W. Ludwig, “Classification of topological insulators and superconductors in three spatial dimensions,” *Phys. Rev. B* 78, 195125 (2008).
- [8] S.-S. Zhang, C. D. Batista, and G. B. Halász, “Towards Kitaev’s sixteenfold way in honeycomb lattice model,” 2019 (unpublished), arXiv:1910.00601.
- [9] F. H. Claro and G. H. Wannier, “Magnetic subband structure of electrons in hexagonal lattices,” *Phys. Rev. B* 19, 6068 (1979).
- [10] D. A. Ivanov, “Non-Abelian Statistics of Half-Quantum Vortices in  $p$ -Wave Superconductors,” *Phys. Rev. Lett.* 86, 268 (2001).
- [11] N. Read and D. Green, “Paired states of fermions in two dimensions with breaking of parity and time-reversal symmetries and the fractional quantum Hall effect,” *Phys. Rev. B* 61, 10267 (2000).

- [12] J. Bellissard, “Change of the Chern number at band crossings,” 1995 (unpublished), cond-mat/9504030.
- [13] A. Kitaev, “Periodic table for topological insulators and superconductors ,” AIP Conf. Proc. 1134, 22 (2009).
- [14] E. Majorana, *Il Nuovo Cimento* (1924-1942) 14, 171 (1937).
- [15] A. Kitaev, “Periodic table for topological insulators and superconductors ,” AIP Conf. Proc. 1134, 22 (2009).
- [16] L. Savary and L. Balents, ”Quantum spin liquids” *Rep. Prog. Phys.*80 016502 (2017).
- [17] D. J. Thouless, M. Kohmoto, P. Nightingale, and M. den Nijs, ”Quantized Hall Conductance in a Two-Dimensional Periodic Potential” *Phys. Rev. Lett.* 49 405 (1982).
- [18] M. Kohmoto, ”Topological Invariant and the Quantization of the Hall Conductance” *Ann. Phys. (N.Y.)* 160 355 (1985).
- [19] C. L. Kane and E. J. Mele, ”Z<sub>2</sub> Topological Order and the Quantum Spin Hall Effect” *Phys. Rev. Lett.* 95 146802 (2005);
- [20] C. Caroli, P. G. De Gennes, J. Matricon, ”Bound Fermion states on a vortex line in a type II superconductor” *Physics letters* 10.1016/0031-9163(64)90375-0 (1964).
- [21] E. Grosfeld, A. Stern, ”Electronic transport in an array of quasiparticles in the  $\nu=5/2$  non-Abelian quantum Hall state” *Phys. Rev. B* 73, 201303(R) (2006).
- [22] M. Cheng, R. M. Lutchyn, V. Galitski, and S. Das Sarma, “Splitting of Majorana-Fermion Modes due to Intervortex Tunneling in a  $p_x + ip_y$  Superconductor,” *Phys. Rev. Lett.* 103, 107001 (2009).
- [23] G. E. Volovik, “The Universe in a Helium Droplet,” (Oxford University Press, 2003).
- [24] G. E. Volovik, “An analog of the quantum Hall effect in a superfluid  $^3\text{He}$  film,” *JETP* 67, 1804 (1988).
- [25] G. E. Volovik, “Fermion zero modes on vortices in chiral superconductors,” *JETP Lett.* 70, 609 (1999).
- [26] V. Lahtinen, “Interacting non-Abelian anyons as Majorana fermions in the honeycomb lattice model,” *New J. Phys.* 13, 075009 (2011).